Cross-Strain Quorum Sensing Inhibition by Staphylococcus aureus. Part 1: A Spatially Homogeneous Model

Jabbari, Sara; King, John R.; Williams, Paul

[Link to publication on Research at Birmingham portal](#)

Cross-strain quorum sensing inhibition by *Staphylococcus aureus.*

Part 1: a spatially homogeneous model.

Sara Jabbari, John R. King

Centre for Mathematical Medicine and Biology, School of Mathematical Sciences, University of Nottingham,

Nottingham, NG7 2RD, UK

Paul Williams

School of Molecular Medical Sciences, University of Nottingham, Nottingham, NG7 2RD, UK

September 6, 2011

Abstract

Staphylococcus aureus uses the *agr* quorum sensing (QS) system to regulate reciprocally colonisation and virulence factor production. *S. aureus* strains can be divided into four *agr* groups: those within a specific *agr* group activate the QS systems of strains belonging to the same group, while inhibiting *agr* expression in strains of other groups. Furthermore, *agr* homologues exist in many more species of Gram-positive bacteria, raising the likelihood of cross-species interference. In principle, a non-pathogenic strain of *S. aureus* or other species of bacteria employing *agr* could be engineered to inhibit the QS systems of pathogenic strains using *agr*, thus down-regulating their production of virulence factors. We present three models of the *agr* operon belonging to strains competing for dominance, each comprising one of the three possible phosphorylation cascades governing the two component system (TCS) of the *agr* system. Bifurcation analyses clarify the aspects of QS most crucial in determining the efficacy of using a non-pathogenic strain for therapeutic purposes if the target TCS cascade is known and illustrate the qualitative and quantitative differences which occur as a result of mechanistic differences between the models. We highlight those results that, in concert

with appropriate experimental data, would be most useful in ascertaining whether or not a classical TCS is in operation in a particular strain if this information is unknown.

Keywords: bifurcation analysis, gene regulation networks, mathematical modelling, quorum sensing, *Staphylococcus aureus*.

1   Introduction

Quorum sensing (QS) is a mechanism for cell-to-cell communication enabling bacterial cells to co-ordinate their behaviour according to their population density. Each bacterial cell produces quorum sensing signal molecules (QSSMs) which accumulate in their local environment. The concentration of these QSSMs can therefore be viewed as a measure of the cells' population density. The bacterial cells sense the QSSMs in their immediate environment and respond to their accumulation by altering the expression of specific genes so facilitating a change in phenotype. Thus unicellular bacteria are able to act collectively as a community rather than simply as individuals. In general, QSSM production is induced by the presence of QSSMs and this positive feedback allows for rapid switching behaviour between two phenotypes.

The specific phenotypes controlled by QS depend upon the species of bacteria. QS was first discovered in the marine bacterium *Vibrio fischeri* which becomes luminescent at high cell population densities [1]. Since then, QS has been found to control many other phenotypes including antibiotic production, motility, biofilm maturation, genetic competence and virulence [2, 3].

Staphylococcus aureus uses QS to regulate reciprocally colonisation and virulence. While its population size is small, *S. aureus* produces surface proteins that facilitate adherence to host tissues and uptake to host cells which aids immune evasion [2]. As the population grows, a switch to the production of secreted virulence factors occurs, leading to the damage and degradation of the surrounding host cells and tissues, thus actively attacking the host. Since tissue damage will alert host defence systems, such a delayed 'deployment tactic' may allow the infecting bacteria time to reach a sufficient population size to be able to overwhelm the host [4].

QS does not mediate communication solely within a population of one species of bacteria, however; it is also manifested as cross-species or cross-strain communication. For example, it has been demonstrated that

Burkholderia cepacia can sense *Pseudomonas aeruginosa* QSSMs in a biofilm [5]. Similarly, there is evidence that the *P. aeruginosa* QSSMs interfere with the QS system of *S. aureus* [6], while strains of *S. aureus* can communicate with one another. Each strain of *S. aureus* is placed into one of four distinct *agr* (accessory gene regulator) categories, groups I-IV. The QSSMs from the strains in each group activate the QS systems of other members of the same group, but inhibit the *agr* systems in the strains from the remaining three *agr* groups [7]. It has also been demonstrated that *Staphylococcus epidermidis* can inhibit *S. aureus* groups I-III, while group IV *S. aureus* strains are the only ones capable of interfering with the QS system of *S. epidermidis* [8, 9].

Such cross-strain or cross-species competition presumably enables the bacteria that invade first to establish their dominance over strains making further attempts at colonisation and infection. Such competition could potentially be used for therapeutic purposes: a non-pathogenic strain could be genetically engineered with a cross group inhibitory QSSM analogue such as that described by McDowell *et al.* [10] so preventing the expression of exotoxin virulence factors. Given the autoregulatory nature of the QS system, the construction of a strain producing an inhibitory QSSM is likely to be more efficient than simply adding the relevant QSSM. Down-regulation of virulence within the pathogen population would allow the host's immune system an increased chance of eliminating the organism. The emergence of multi-antibiotic resistant *S. aureus* (including methicillin- and vancomycin-resistant *S. aureus*, MRSA and VRSA respectively) means that understanding the virulence mechanisms employed by this pathogen to cause disease should aid the development of novel therapies, such as that mentioned above, to combat infection through attenuation of virulence.

The *agr* operon was first discovered in *S. aureus* [11] but has since been identified in many other Gram-positive bacteria, including the pathogens *Clostridium botulinum* [12], *Clostridium perfringens* [13], *Enterococcus faecaelis* [14] and *Listeria monocytogenes* [15]. In *S. aureus*, the operon consists of two divergent promoters termed P2 and P3. The P3 transcript encodes a regulatory mRNA, RNAIII. Increased levels of RNAIII result in increased translation of secreted virulence factors and repression of surface protein production [16]. RNAIII is essentially the effector of the *agr* operon, a regulatory molecule that induces the desired *agr* phenotype. The P2 promoter controls the QS loop that regulates the activity of both promoters (see Figure 1), producing the proteins AgrA, AgrB, AgrC and AgrD. AgrB and AgrC are transmembrane proteins, i.e. after translation, these proteins move into the membrane of the *S. aureus* cell, while AgrD is anchored to the membrane. AgrB
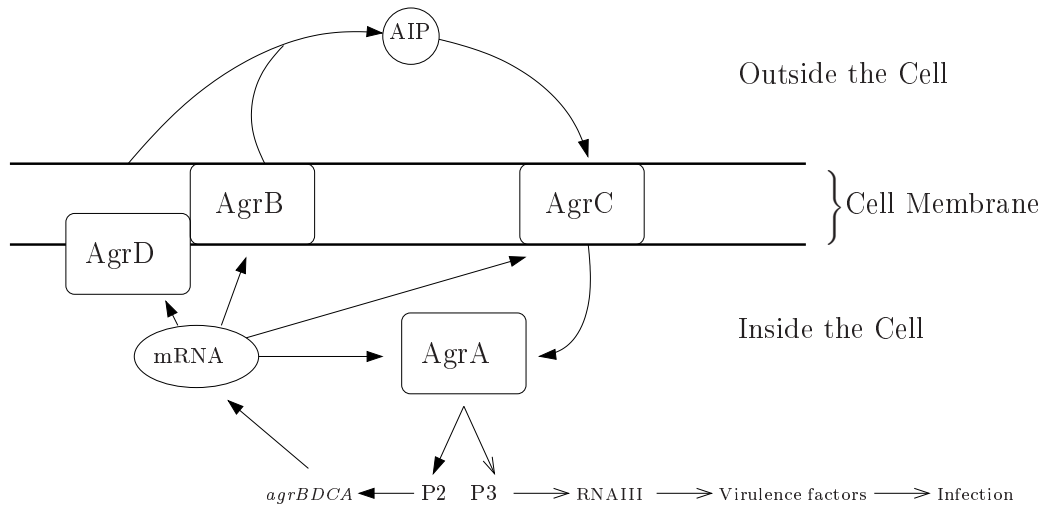
Figure 1: A schematic of the *agr* positive feedback loop (arrows with a filled head) and its downstream effects. The trigger of the loop is the accumulation of AIP in the environment of the cell.

is a membrane associated enzyme which processes the linear AgrD pro-peptide to generate and export out of the cell the active QSSM (i.e., AgrB facilitates the conversion of intracellular AgrD into extracellular QSSM), a cyclic peptide termed the 'autoinducing peptide' (AIP) [17, 18]. The AgrA and AgrC proteins form a signal transduction system called a two-component system (TCS). A TCS consists of a membrane associated receptor protein (here AgrC) and a response regulatory DNA-binding protein inside the cell (AgrA). The receptor detects the QSSM signal (i.e. the AIP binds to AgrC) and communicates this to the response regulator, which then influences the transcription of the target genes (here activated AgrA upregulates the transcription of the *agrBDCA* operon as well as RNAIII-dependent and RNAIII-independent genes [19]).

The structural identity of the AIP molecules of the strains within a given group of *S. aureus* enables a particular strain to activate the QS systems of all others within its group. The structural differences between groups, on the other hand, provide a natural inhibition process: the AIP molecules are sufficiently similar that they will bind to the AgrC receptor proteins of any strain, but if they bind to an AgrC receptor from an opposition group they will not confer the ability to activate the AgrA protein inside the cell, thus effectively blocking the QS loop and potentially forcing the cells into, or maintaining them in, a down-regulated state where the exotoxins are not produced.

AgrA is activated by AgrC via a phosphorylation cascade. In a classical TCS, the receptor autophospho-

4

rylates on detection of the signal and transfers this phosphate to the regulator. The phosphorylated regulator usually has a higher affinity for the relevant DNA binding site(s) (here, P2 and P3). While much work has been done on defining the *agr* system, a question mark remains over the mechanisms governing this phosphorylation cascade in all strains and species that use *agr*. It has been shown in laboratory derivatives of *S. aureus* that AgrC does indeed autophosphorylate [20], implying that in this case it functions as a classical TCS. However, given the variety of TCSs in existence in the bacterial kingdom [21], suggestions that both AgrA and AgrC could be phosphorylated constitutively in [11] and experimental evidence that AgrA can bind the relevant DNA binding site in either its phosphorylated or its unphosphorylated form (though it has a higher affinity in the former case) in [22] open up the possibility that the phosphorylation cascade may vary within and between strains (the variations in *agr* systems and their functions between species is discussed in [23]).

Though models of interacting QS systems exist for Gram-negative bacteria (see, for example, [24] or [25]), equivalent models of Gram-positive systems are lacking. Given the importance of fully understanding the *agr* operon before it can be exploited for therapeutic gain, we here focus on cross-strain competitive QS with a view to (i) identifying aspects of the *agr* system which are most influential in inactivating an opposition strain; and (ii) identifying potential experiments and/or behaviour which could be used to determine the AgrC-AgrA phosphorylation cascade in operation in a particular strain of *S. aureus* (or, likewise, in any other bacteria employing an *agr* operon). In consideration of these points, we present three models of cross-strain *agr* competition, each representing one of the three possible phosphorylation cascades in the TCS. These models have been analysed in the single-strain case in [26], wherein the TCSs are subject to artificial inhibitor AIP molecules. Descriptions of the three models are given below.

- Model I: the classical TCS.

    The receptor (transmembrane AgrC) autophosphorylates on detection of the signal (i.e. on binding to an AIP molecule), followed by a phosphotransfer to the response regulator (AgrA). The phosphorylated response regulator has a higher affinity for the promoter sites than its non-phosphorylated counterpart.

- Model II: the response regulator is constitutively phosphorylated by kinases.
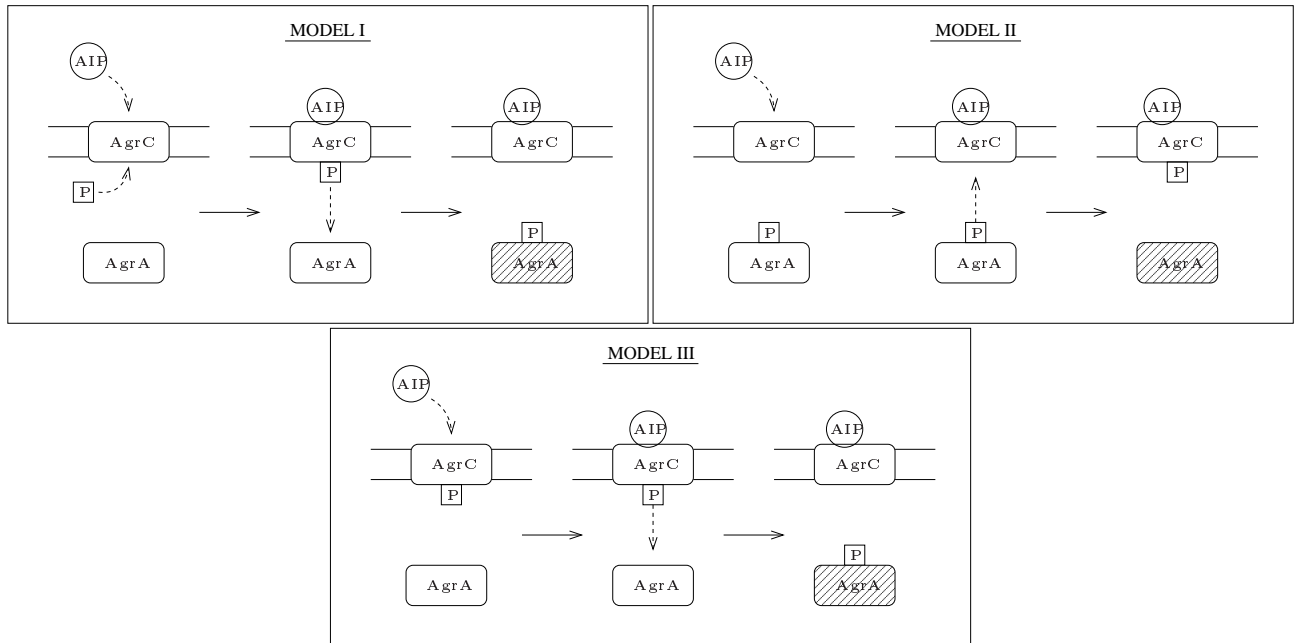
Figure 2: A schematic of the three different possibilities for the phosphorylation cascade of the TCS of the *agr* operon (the small square represents a phosphate and the activated form of AgrA is in each case shown shaded). Model I follows the classical TCS. In Model II AgrA is constitutively phosphorylated and consequently it is dephosphorylated AgrA which takes on the role of activator. In Model III transmembrane AgrC is phosphorylated in the absence of AIP; upon binding to an AIP molecule it transfers this phosphate to the AgrA protein, leaving phosphorylated AgrA as the activator.

> In this case detection of the signal results in a phosphotransfer from the response regulator to the receptor. The dephosphorylated response regulator thus serves as the activator in this model.

- Model III: the receptor is constitutively phosphorylated by kinases.

> On detection of the signal, the receptor transfers this phosphate to the response regulator. As with Model I, it is then the phosphorylated response regulator that is the activator.

Figure 2 illustrates graphically each of these putative phosphorylation cascades. Unfortunately, a specific cascade has yet to be identified definitively in any *agr* operon, though experimental evidence that AgrC autophosphorylates [20] and that phosphorylated AgrA has a high binding affinity with the P2 promoter region lends weight to the classical TCS (Model I) in the strains which have been studied. Given the relative ease of

6

testing hypotheses theoretically and the possible variation between strains and species, all three of these models should be examined (moreover, since there must be phosphotransfer between AgrC and AgrA, these three are the only possibilities).

Analysis of the mathematical models in [26] illustrated that the sensitivity of these three different TCSs to inhibition (i.e., the level of treatment required to inactivate the *agr* operon) via the addition of synthetic inhibitor molecules was highly dependent upon the phosphorylation cascade: Model I was the most robust and Model II the most sensitive. In addition, each model displayed bistable behaviour in response to inhibitor molecule dosage, suggesting that such an approach to inactivate the *agr* operon may only be successful if the infection is caught sufficiently early, otherwise potentially impractical levels of inhibitor molecules are required. A natural extension of this is therefore to consider a competing strain (rather than competing molecules). We focus here on three nondimensional parameters that we believe to be of substantial importance in determining the outcome of the competition between two strains, rather than between a strain and inhibitor molecules; these parameters are the relative population sizes and the relative rates of self-activation binding and of inhibitory binding between receptors and AIPs, principally because these are the parameters most easily specified in reality, either through the treatment dosage or through the design of the therapeutic strain. We explore the responses of the models to variations in these three parameters with the aim of finding parameter sets where one strain can be reliably down-regulated. We demonstrate that the system behaviour in response to alteration in the binding rates can be counter-intuitive and that the most reliable parameter to modulate in order to achieve downregulation of an opposition population is the relative population size.

2 Formulation

2.1 Variables and Parameters

In [27], the *agr* operon was modelled in the absence of any competition (i.e. neither an opposing strain nor synthetic inhibitor molecules) and a time-dependent asymptotic analysis was performed to highlight the mechanisms involved in each stage of activation of the operon and to derive simpler models which could be used to analyse further various processes. In this study, we formulate a model of two competitive strains of *S.*

Models I,II and III	
M_j	mRNA in Population j
$A_j, ..., D_j$	cytoplasmic AgrA, ..., AgrD in Population j
T_j, R_j	transmembrane AgrB, AgrC in Population j
S_j	anchored AgrD in Population j
a_j	free AIP from Population j
A_{Pj}	phosphorylated AgrA in Population j
P_j	proportion of cells that is up-regulated in Population j
Models I and II	
$R_{Pj}^{a_j}$	(Phosphorylated) receptor bound to cognate AIP in Population j
$R_j^{a_l}$	(Non-phosphorylated) receptor in Population j bound to opposition AIP from Population l
Model III	
$R_{Pj}^{a_j}$	(Phosphorylated) receptor bound to cognate AIP in Population j
$R_{Pj}^{a_l}$	(Phosphorylated) receptor in Population j bound to opposition AIP from Population l
$R_j^{a_j}$	De-phosphorylated receptor bound to cognate AIP in Population j

Table 1: Definitions of the variables, with $j = 1, 2$ and $l = 3 - j$.

aureus termed Population 1 and Population 2 and in the absence of one of the populations the models reduce to those of [27]. Thus, we focus the description here on the cross-species interaction terms and the reader may refer to [27] for additional model assumptions and derivations. We require variables to represent the amount of mRNA, proteins etc. in two separate populations. We therefore let $X_1(t)$ and $X_2(t)$ represent the amount of X in Population 1 and Population 2 respectively. The resulting variables are displayed in Table 1.

The models necessarily contain a large number of parameters and as a matter of expedience we assume the parameters governing corresponding reactions in the two populations are equal, i.e. the two populations perform all reactions at equal rates. The only exceptions are the parameters representing population sizes and the rates of association and dissociation. It is the AIP structure which determines group specificity and the latter two rates are accordingly the most likely to differ between groups. Definitions of the parameters are given in Table
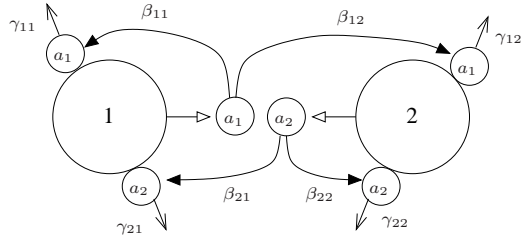
Figure 3: A schematic of two bacteria from opposing staphylococcal groups (Population 1 and Population 2) with their respective AIP (a_1 and a_2), illustrating the parameters in the model that represent the different binding and unbinding reactions between the AIP and receptors of each population. β_{11} and β_{22} are self-activating rates, while β_{12} and β_{21} are cross-inhibiting binding rates. γ_{11} and γ_{22} are the rates of dissociation of AIP from its cognate receptor and γ_{12} and γ_{21} from its opposition receptor.

2. Figure 3 illustrates which AIP binding rates and which dissociation rates correspond to either self-activation or cross-inhibition.

We assume that the two populations are in a (well-mixed) spatially homogeneous environment (a spatially structured extension of this model is discussed in Part 2 of this study [28]).

Parameter	Rate constant for	Unit
m	basal production of mRNA	molecules cells^{-1} s^{-1}
v	QS-induced mRNA transcription	molecules cells^{-1} s^{-1}
κ	protein translation	s^{-1}
$\alpha_{T,R}$	AgrB and C taken up into cell membrane	s^{-1}
α_S	AgrD anchors to cell membrane	s^{-1}
λ_X	natural degradation of variable $X(t)$	s^{-1}
r	dilution through cell division	s^{-1}
δ_X	$\lambda_X + r$	s^{-1}
k	AIP production from AgrD, mediated by AgrB	molecules^{-1} cm^3 s^{-1}
ϕ	activation of AgrA by AIP-bound receptor	molecules^{-1} cm^3 s^{-1}
μ	dephosphorylation of AgrA by phosphatases	s^{-1}
b	binding of the promoter site	molecules^{-1} cells s^{-1}
u	unbinding of the promoter site	s^{-1}
ψ_A	AgrA phosphorylation on production (Model II only)	s^{-1}
ψ_R	AIP-independent phosphorylation of transmembrane AgrC (Model III only)	s^{-1}
β_{jl}	AIP from Population j binding to Population l receptors	molecules^{-1}cm^{3}s^{-1}
γ_{jl}	AIP from Population j disassociating from Population l receptors	s^{-1}
N_j	total number of bacteria per unit volume from Population j	cells cm^{-3}

Table 2: Definitions of the parameters, with $j = 1, 2$ and $l = 3 - j$. All parameters except N_j are rate constants.

2.2 Model I - the classical TCS

2.2.1 Dimensional model

The dimensional model reads, with $j = 1, 2$ and $l = 3 - j$,

$$\frac{dM_j}{dt} = N_j m + N_j v P_j - \delta_M M_j, \tag{1}$$

$$\frac{dA_j}{dt} = \kappa M_j - \phi A_j R_{P_j}^{a_j} + \mu A_{Pj} - \delta_A A_j, \tag{2}$$

$$\frac{dB_j}{dt} = \kappa M_j - (\alpha_T + \delta_B) B_j, \tag{3}$$

$$\frac{dC_j}{dt} = \kappa M_j - (\alpha_R + \delta_C) C_j, \tag{4}$$

$$\frac{dD_j}{dt} = \kappa M_j - (\alpha_S + \delta_D) D_j, \tag{5}$$

$$\frac{dS_j}{dt} = \alpha_S D_j - \delta_S S_j - k T_j S_j, \tag{6}$$

$$\frac{dT_j}{dt} = \alpha_T B_j - \delta_T T_j, \tag{7}$$

$$\frac{da_j}{dt} = k T_j S_j - \beta_{jj} R_j a_j + \gamma_{jj} R_{P_j}^{a_j} - \beta_{jl} R_l a_j + \gamma_{jl} R_l^{a_j} - \lambda_a a_j, \tag{8}$$

$$\frac{dR_j}{dt} = \alpha_R C_j - \beta_{jj} R_j a_j + \gamma_{jj} R_{P_j}^{a_j} - \beta_{lj} R_j a_l + \gamma_{lj} R_j^{a_l} - \delta_R R_j, \tag{9}$$

$$\frac{dR_{P_j}^{a_j}}{dt} = \beta_{jj} R_j a_j - (\gamma_{jj} + \delta_{R^a}) R_{P_j}^{a_j}, \tag{10}$$

$$\frac{dR_j^{a_l}}{dt} = \beta_{lj} R_j a_l - (\gamma_{lj} + \delta_{R^a}) R_j^{a_l}, \tag{11}$$

$$\frac{dA_{Pj}}{dt} = \phi A_j R_{P_j}^{a_j} - (\mu + \delta_{A_P}) A_{Pj}, \tag{12}$$

$$\frac{dP_j}{dt} = \frac{b}{N_j} A_{Pj} (1 - P_j) - u P_j. \tag{13}$$

As for the single-species model in [26, 27], we take the default initial conditions to be the naturally down-regulated steady states, i.e. the steady-state solutions to (1)-(13) with $k = 0$ or, equivalently, as $\lambda_a \to \infty$ (these

are not the same as the down-regulated steady states caused by suppression from opposition bacteria). Thus,

$$a_j(0) = R_{P_j}^{a_j}(0) = R_j^{a_l}(0) = A_{Pj}(0) = P_j(0) = 0,$$

$$M_j(0) = \frac{N_j m}{\delta_M}, \qquad A_j(0) = \frac{N_j \kappa m}{\delta_M \delta_A}, \qquad B_j(0) = \frac{N_j \kappa m}{\delta_M(\alpha_T + \delta_B)},$$

$$C_j(0) = \frac{N_j \kappa m}{\delta_M(\alpha_R + \delta_C)}, \qquad D_j(0) = \frac{N_j \kappa m}{\delta_M(\alpha_S + \delta_D)}, \qquad R_j(0) = \frac{N_j \alpha_R \kappa m}{\delta_M \delta_R(\alpha_R + \delta_C)},$$

$$S_j(0) = \frac{N_j \alpha_S \kappa m}{\delta_M \delta_S(\alpha_S + \delta_D)}, \quad T_j(0) = \frac{N_j \alpha_T \kappa m}{\delta_M \delta_T(\alpha_T + \delta_B)}.$$

(14)

2.2.2 Nondimensional model

The variables are nondimensionalised using the same principles used for the single population model in [26]. The nondimensionalisation of opposition-bound receptors (the only variable to not have a direct match in the single population model) is chosen to simplify the corresponding equation. The nondimensional variables are thus:

$$M_j' = \frac{\delta_M}{N_j m} M_j, \qquad\qquad A_j' = \frac{\delta_M \delta_A}{N_j \kappa m} A_j,$$

$$a_j' = \frac{\beta_{jj} \phi b N_j \alpha_R \kappa^2 m^2}{\delta_M{}^5 \delta_A \delta_R(\alpha_R + \delta_C)} a_j, \quad R_{P_j}^{a_j}{}' = \frac{\phi b \kappa m}{\delta_M{}^3 \delta_A} R_{P_j}^{a_j},$$

(15)

$$R_j^{a_l}{}' = \frac{\beta_{ll} \phi b N_l \kappa m}{\beta_{lj} N_j \delta_M{}^3 \delta_A} R_j^{a_l}, \qquad A_{Pj}{}' = \frac{b}{N_j \delta_M} A_{Pj}, \qquad \tau = \delta_M t,$$

and

$$\left.\begin{array}{l} X_j' = \dfrac{\delta_M(\alpha_Y + \delta_X)}{N_j \kappa m} X_j \\[4mm] Y_j' = \dfrac{\delta_M(\alpha_Y + \delta_X)\delta_Y}{N_j \alpha_Y \kappa m} Y_j \end{array}\right\} \quad \text{for } (X,Y) = (B,T), (C,R) \text{ or } (D,S).$$

(16)

We define the nondimensional parameters

$$N = \frac{N_1}{N_2}, \qquad \beta_A = \frac{\beta_{22}}{\beta_{11}}, \qquad \beta_I = \frac{\beta_{12}}{\beta_{21}}.$$

(17)

We refer to these as the ratio of population sizes, self-activation rates and cross-inhibition rates, respectively.

In order to incorporate these ratios into the model, we define the following nondimensional parameters:

$$\lambda_a' = \frac{\lambda_a}{\delta_M}, \quad v' = \frac{v}{m}, \quad \beta_{11}' = \frac{\beta_{11}\tilde{R}_1}{\delta_M}, \quad \beta_{21}' = \frac{\beta_{21}\tilde{R}_1}{\delta_M}, \quad \eta = \frac{N_1\beta_{11}\delta_M}{\phi b \tilde{A}_1},$$

$$u' = \frac{u}{\delta_M}, \quad \mu' = \frac{\mu}{\delta_M}, \quad \phi' = \frac{N_1\delta_M}{b\tilde{A}_1}, \quad k_S = \frac{k\tilde{T}_1}{\delta_M}, \quad \gamma_{[11,22,12,21]}' = \frac{\gamma_{[11,22,12,21]}}{\delta_M}, \tag{18}$$

$$k_a = \frac{k\beta_{11}\phi b \tilde{A}_1 \tilde{T}_1 \tilde{R}_1 \tilde{S}_1}{N_1\delta_M^4},$$

(these also follow directly from [26]) where $\tilde{X}$ is the initial condition of X given by (14) for $X = A_1, T_1, R_1, S_1$; finally we set

$$\lambda_X' = \frac{\delta_X}{\delta_M} \qquad \text{for} \quad X = A_j, T_j, R_j, S_j, A_{Pj}, RP_j^{a_j}, R_j^{a_j},$$

$$\alpha_{X,Y}' = \frac{\delta_X + \alpha_Y}{\delta_M} \quad \text{for} \quad (X,Y) = (B_j, T_j), (C_j, R_j) \text{ or } (D_j, S_j). \tag{19}$$

Assuming that protein degradation rates, λ_X in (19), are negligible relative to r (and since $\delta_X = \lambda_X + r$), we set all the parameters in (19) to be equal. Thus

$$\lambda_X' = \lambda \qquad \text{for} \quad X = A_j, T_j, R_j, S_j, A_{Pj}, RP_j^{a_j}, R_j^{a_j},$$

$$\alpha_{X,Y}' = \alpha \quad \text{for} \quad (X,Y) = (B_j, T_j), (C_j, R_j) \text{ or } (D_j, S_j), \tag{20}$$

($j = 1, 2$ and $l = 3 - j$ respectively).

Default parameter values are those adopted in [26] (with the new cross-strain binding and dissociation rates taken to be of the same order as the equivalent cognate rates), namely

$$k_S = \epsilon \hat{k}_S, \quad \mu' = \epsilon \hat{\mu}, \quad v' = \frac{1}{\epsilon}\hat{v}, \quad \beta_{11}' = \frac{1}{\epsilon}\hat{\beta}_{11}, \quad \beta_{21}' = \frac{1}{\epsilon}\hat{\beta}_{21}, \quad k_a = \frac{1}{\epsilon^2}\hat{k}_a, \quad \psi_A' = \frac{1}{\epsilon^2}\hat{\psi}_A, \tag{21}$$

where $\epsilon = m/v$, i.e. the ratio of basal transcription to QS-induced transcription; hatted parameters are all $O(1)$ and will be set to unity in the simulations. Detailed explanations of this parameter choice are provided in [26, 27], alongside a discussion of the consequences of alternative parameter choices. We summarise briefly our reasoning here.

- It is vital that ϵ be small in order that the cells can induce rapidly the QS-associated switch between down- and up-regulated states which is known to arise. Similarly (for Model II only), constitutive phosphorylation of AgrA must be sufficiently fast for this to be achieved.

- Signal transduction reactions should occur at a fast rate relative to general reactions such as transcription and translation (examination of the nondimensional definition of k_a in (18) shows why this this assumption also results in k_a being large).

(a)	Nondimensional parameter	Default value
	ϵ	0.1
	k_S, μ	0.1
	$\alpha, \lambda, \lambda_a, \eta, \gamma_{11}, \gamma_{22}, \gamma_{12}, \gamma_{21}, \phi, \psi_R, \zeta, u$	1
	$v, \beta_{11}, \beta_{21}$	10
	k_a, ψ_A	100

(b)	Nondimensional parameter	Default value
	ϵ	0.05
	k_S, η, μ	0.05
	$\alpha, \lambda, \lambda_a, \eta, \gamma_{11}, \gamma_{22}, \gamma_{12}, \gamma_{21}, \phi, \psi_R, \zeta, u$	1
	$v, \beta_{11}, \beta_{21}$	20
	k_a, ψ_A	200

Table 3: The default parameter set for the non-hatted parameters for two values of ϵ (all hatted parameters are unity). In this paper we focus on the effect of varying N, β_A and β_I. In general we use (a) $\epsilon = 0.1$ and thus the top parameter set. However, we have also used (b) $\epsilon = 0.05$ in Figures 4-6 to demonstrate the results for smaller ϵ, in which case the parameters follow from (b).

- Housekeeping dephosphorylation of AgrA is relatively slow as an efficient cell should be well-equipped to manage with little of this process.

We remark that $k_S = O(1)$ was employed in [27] in order to simplify the asymptotic analysis; however, we here return to the biologically-motivated scaling employed in [26, 29] ($k_S = O(\epsilon)$). Notice that ψ_A appears in Model II only and so the definition of ψ_A' is given in §2.3.1, though its size is given above in (21). All hatted parameters and the remaining nondimensional parameters which are not listed in (21) are taken to be $O(1)$, and in all simulations we set them to unity: the default parameter values are given in Table 3.

Dropping $'$s, the nondimensional equations for Model I are:

$$\frac{dM_j}{d\tau} = \frac{1}{\epsilon}\hat{v}P_j - M_j + 1, \tag{22}$$

$$\frac{dA_j}{d\tau} = \lambda(M_j - A_j) - \phi A_j R_{Pj}^{a_j} + \epsilon\hat{\mu}\phi A_{Pj}, \tag{23}$$

$$\frac{dB_j}{d\tau} = \alpha(M_j - B_j), \tag{24}$$

$$\frac{dC_j}{d\tau} = \alpha(M_j - C_j), \tag{25}$$

$$\frac{dD_j}{d\tau} = \alpha(M_j - D_j), \tag{26}$$

$$\frac{dS_1}{d\tau} = \lambda(D_1 - S_1) - \epsilon\hat{k}_S T_1 S_1, \tag{27}$$

$$\frac{dS_2}{d\tau} = \lambda(D_2 - S_2) - \epsilon\frac{\hat{k}_S}{N}T_2 S_2, \tag{28}$$

$$\frac{dT_j}{d\tau} = \lambda(B_j - T_j), \tag{29}$$

$$\frac{da_1}{d\tau} = \frac{1}{\epsilon^2}\hat{k}_a T_1 S_1 - \frac{1}{\epsilon}\hat{\beta}_{11} R_1 a_1 + \frac{1}{\epsilon}\hat{\beta}_{11}\gamma_{11} R_1^{a_1} - \frac{1}{\epsilon}\frac{\beta_I\hat{\beta}_{21}}{N} R_2 a_1 + \frac{1}{\epsilon}\frac{\beta_I\hat{\beta}_{21}\gamma_{12}}{N} R_2^{a_1} - \lambda_a a_1, \tag{30}$$

$$\frac{da_2}{d\tau} = \frac{1}{\epsilon^2}\frac{\beta_A\hat{k}_a}{N^3} T_2 S_2 - \frac{1}{\epsilon}\frac{\beta_A\hat{\beta}_{11}}{N} R_2 a_2 + \frac{1}{\epsilon}\frac{\beta_A\hat{\beta}_{11}\gamma_{22}}{N} R_2^{a_2} - \frac{1}{\epsilon}\hat{\beta}_{21} R_1 a_2 + \frac{1}{\epsilon}\hat{\beta}_{21}\gamma_{21} R_1^{a_2} - \lambda_a a_2, \tag{31}$$

$$\frac{dR_1}{d\tau} = \lambda(C_1 - R_1) - \epsilon\frac{\eta}{\hat{\beta}_{11}} R_1 a_1 + \epsilon\frac{\eta\gamma_{11}}{\hat{\beta}_{11}} R_{P1}^{a_1} - \epsilon\frac{N\hat{\beta}_{21}\eta}{\beta_A\hat{\beta}_{11}^2} R_1 a_2 + \epsilon\frac{N\hat{\beta}_{21}\eta\gamma_{21}}{\beta_A\hat{\beta}_{11}^2} R_1^{a_2}, \tag{32}$$

$$\frac{dR_2}{d\tau} = \lambda(C_2 - R_2) - \epsilon N\frac{\eta}{\hat{\beta}_{11}} R_2 a_2 + \epsilon\frac{N\eta\gamma_{22}}{\hat{\beta}_{11}} R_{P2}^{a_2} - \epsilon\frac{\beta_I\hat{\beta}_{21}\eta}{\hat{\beta}_{11}^2} R_2 a_1 + \epsilon\frac{\beta_I\hat{\beta}_{21}\eta\gamma_{12}}{\hat{\beta}_{11}^2} R_2^{a_1}, \tag{33}$$

$$\frac{dR_{Pj}^{a_j}}{d\tau} = R_j a_j - (\lambda + \gamma_{jj})R_{Pj}^{a_j}, \tag{34}$$

$$\frac{dR_j^{a_l}}{d\tau} = R_j a_l - (\lambda + \gamma_{lj})R_j^{a_l}, \tag{35}$$

$$\frac{dA_{Pj}}{d\tau} = A_j R_{Pj}^{a_j} - (\lambda + \epsilon\hat{\mu})A_{Pj}, \tag{36}$$

$$\frac{dP_j}{d\tau} = A_{Pj}(1 - P_j) - uP_j, \tag{37}$$

with the initial conditions:

$$M_j(0) = A_j(0) = B_j(0) = C_j(0) = D_j(0) = S_j(0) = T_j(0) = R_j(0) = 1,$$
$$a_j(0) = R_{Pj}^{a_j}(0) = R_j^{a_l}(0) = A_{Pj}(0) = P_j(0) = 0. \tag{38}$$

Notice that the equations representing the two populations are not symmetric in terms of the dimensionless parameters because, to incorporate (17) into the system, the nondimensional parameters in (18) are chosen to be dependent upon the dimensional N_1, β_{11} and β_{21}, but not upon N_2, β_{22} or β_{12}. For this reason, the bifurcation diagrams will not be symmetric about the points where the two populations are equivalent (i.e. $N = 1$, $\beta_A = 1$ and $\beta_I = 1$).

2.3 Model II - AgrA is constitutively phosphorylated

2.3.1 Nondimensional model

In the interest of space, the dimensional Models II and III and the details of their nondimensionalisations (which are largely the same as that of Model I) are relegated to the appendix. We present here the nondimensional models only. The nondimensional Model II (dropping $''$'s) is given by (22), (24)-(35) and

$$\frac{dA_j}{dt} = \lambda(M_j - A_j) - \hat{\psi}_A A_j + \phi^2 A_{Pj} R_{Pj}^{a_j} + \hat{\mu}\phi A_{Pj}, \tag{39}$$

$$\frac{dA_{Pj}}{dt} = \frac{\hat{\psi}_A}{\phi} A_j - \phi A_{Pj} R_{Pj}^{a_j} - (\lambda + \hat{\mu})A_{Pj}, \tag{40}$$

$$\frac{dP_j}{dt} = \frac{1}{\phi} A_j(1 - P_j) - uP_j. \tag{41}$$

The initial conditions which differ from (38) are

$$A_j(0) = \frac{\hat{\mu} + \lambda}{\hat{\mu} + \lambda + \hat{\psi}_A}, \quad A_{Pj}(0) = \frac{\hat{\psi}_A}{\phi(\hat{\mu} + \lambda + \hat{\psi}_A)}, \quad P_j(0) = \frac{\hat{\mu} + \lambda}{\hat{\mu} + \lambda + \phi u(\hat{\mu} + \lambda + \hat{\psi}_A)}. \tag{42}$$

The hatted parameters are scaled according to (21).

2.4 Model III - AgrC is constitutively phosphorylated

2.4.1 Nondimensional model

The nondimensional Model III is given by (22)-(29), (36), (37) and

$$\frac{da_1}{d\tau} = \frac{1}{\epsilon^2}\hat{k}_a T_1 S_1 - \frac{1}{\epsilon}\hat{\beta}_{11} R_{P1} a_1 + \frac{1}{\epsilon^2}\frac{\hat{\beta}_{11}^2\gamma_{11}}{\eta\zeta}R_1^{a_1} + \frac{1}{\epsilon}\hat{\beta}_{11}\gamma_{11}R_{P1}^{a_1} - \frac{1}{\epsilon}\frac{\beta_I\hat{\beta}_{21}}{N}R_{P2}a_1$$
$$+ \frac{1}{\epsilon}\frac{\beta_I\hat{\beta}_{21}\gamma_{12}}{N}R_{P2}^{a_1} - \lambda_a a_1, \tag{43}$$

$$\frac{da_2}{d\tau} = \frac{1}{\epsilon^2}\frac{\beta_A\hat{k}_a}{N^3}T_2 S_2 - \frac{1}{\epsilon}\frac{\beta_A\hat{\beta}_{11}}{N}R_{P2}a_2 + \frac{1}{\epsilon^2}\frac{\beta_A\hat{\beta}_{11}^2\gamma_{22}}{N^2\eta\zeta}R_2^{a_2} + \frac{1}{\epsilon}\frac{\beta_A\hat{\beta}_{11}\gamma_{22}}{N}R_{P2}^{a_2} - \frac{1}{\epsilon}\hat{\beta}_{21}R_{P1}a_2$$
$$+ \frac{1}{\epsilon}\hat{\beta}_{21}\gamma_{21}R_{P1}^{a_2} - \lambda_a a_2, \tag{44}$$

$$\frac{dR_j}{d\tau} = (\psi_R + \lambda)(C_j - R_j) + \frac{\gamma_{jj}\psi_R}{\lambda\zeta}R_j^{a_j}, \tag{45}$$

$$\frac{dR_{P1}}{d\tau} = \lambda(R_1 - R_{P1}) - \epsilon\frac{\eta}{\hat{\beta}_{11}}R_{P1}a_1 + \epsilon\frac{\eta\gamma_1}{\hat{\beta}_{11}}R_{P1}^{a_1} - \epsilon\frac{N\hat{\beta}_{21}\eta}{\beta_A\hat{\beta}_{11}^2}R_{P1}a_2 + \epsilon\frac{N\hat{\beta}_{21}\eta\gamma_{21}}{\beta_A\hat{\beta}_{11}^2}R_{P1}^{a_2}, \tag{46}$$

$$\frac{dR_{P2}}{d\tau} = \lambda(R_2 - R_{P2}) - \epsilon\frac{N\eta}{\hat{\beta}_{11}}R_{P2}a_2 + \epsilon\frac{N\eta\gamma_{22}}{\hat{\beta}_{11}}R_{P2}^{a_2} - \epsilon\frac{\beta_I\hat{\beta}_{21}\eta}{\hat{\beta}_{11}^2}R_{P2}a_1 + \epsilon\frac{\beta_I\hat{\beta}_{21}\eta\gamma_{12}}{\hat{\beta}_{11}^2}R_{P2}^{a_1}, \tag{47}$$

$$\frac{dR_{P1}^{a_1}}{d\tau} = R_{P1}a_1 - \frac{1}{\epsilon}\frac{\hat{\beta}_{11}}{\eta\zeta}A_1 R_{P1}^{a_1} - (\lambda + \gamma_{11})R_{P1}^{a_1}, \tag{48}$$

$$\frac{dR_{P2}^{a_2}}{d\tau} = R_{P2}a_2 - \frac{1}{\epsilon}\frac{\hat{\beta}_{11}}{N\eta\zeta}A_2 R_{P2}^{a_2} - (\lambda + \gamma_{22})R_{P2}^{a_2}, \tag{49}$$

$$\frac{dR_{Pj}^{a_l}}{d\tau} = R_{Pj}a_l - (\lambda + \gamma_{lj})R_{Pj}^{a_l}, \tag{50}$$

$$\frac{dR_j^{a_j}}{d\tau} = A_j R_{Pj}^{a_j} - (\lambda + \gamma_{jj})R_j^{a_j}. \tag{51}$$

The nondimensional initial conditions which differ from (38) are

$$R_{Pj}(0) = 1, \quad R_{Pj}^{a_l}(0) = 0, \quad R_j^{a_j}(0) = 0. \tag{52}$$

The hatted parameters are scaled according to (21) (note that primes have been dropped from the derivation details provided in the appendix).

3 Numerical investigations

3.1 Preliminaries

When $N = \beta_A = \beta_I = 1$ the two populations of cells behave identically, i.e. they result in matching levels of regulation and of all corresponding proteins. We look at how altering these three parameters can affect the

solutions of the models with a view to identifying properties of the system which should enable one population to downregulate the other. We track the solution curves in response to varying N, β_A and β_I, focusing primarily on $N, \beta_I > 1$ and $\beta_A < 1$, with the expectation that in these regimes Population 1 should be 'stronger' than Population 2, by which we mean in a better position to inactivate Population 2. Mathematically speaking, Population 1 inactivating or downregulating Population 2 would be given by $\bar{P}_1 \sim 1$ and $\bar{P}_2 << 1$ since $\bar{P}_1$ is the steady state proportion of up-regulated cells in Population 1 and $\bar{P}_2$ that of Population 2. Our investigations indicate, however, that these values can in fact vary significantly from 1 or 0, so we take the rather informal description that Population 1 has inactivated or down-regulated Population 2 if $\bar{P}_2 < 0.5$ and $\bar{P}_1 > 0.5$ is significantly larger than $\bar{P}_2$ (on [0 1]).

We will see that five cases emerge from our analyses, each representing a different situation regarding the potential ability of one population to downregulate the other. Given the number of possibilities, to make the qualitative conclusions clearer to the reader, we summarise these in Table 4 rather than introducing each case as it arises. Two cases are monostable: either both populations are necessarily active (Case V) or Population 1 necessarily inactivates Population 2 (Case W). Two are bistable and the outcome is dependent on initial conditions: in Case X either both become active or Population 1 inactivates Population 2, while in Case Y each population can downregulate the other. Finally, Case Z has tristable behaviour and all of the outcomes mentioned above are possible. Thus when Cases Y and Z arise, the model is displaying what could be deemed to be unexpected behaviour because Population 2 is able to downregulate Population 1 (given suitable initial conditions) despite being 'weaker' in terms of either N, β_A or β_I (remember these are chosen to give Population 1 the advantage in these studies).

In all the bifurcation diagrams below solid lines indicate stable steady states and dashed lines unstable ones. In a number of figures, it is impossible to distinguish between two or more branches visually; when this happens we illustrate the fact that there are multiple branches present using a dot-dash line. In the time-dependent solutions, solid lines illustrate the solution for Population 1 and dashed lines the corresponding solution for Population 2, unless otherwise stated.

Although for completeness we have prescribed initial conditions for the three models in (38), (42) and (52), we often vary these when deriving time-dependent solutions in order to examine any multistable behaviour

		Outcome(s)	
Case	Stability	Population 1	Population 2
V	Mono	active	active
W	Mono	active	inactive
X	Bi	active	active
		active	inactive
Y	Bi	active	inactive
		inactive	active
Z	Tri	active	active
		active	inactive
		inactive	active

Table 4: The five phenotypes that arise from our analysis in §3.2-§3.4 as a result of varying N, β_I (> 1) or β_A (< 1). The expectation might *a priori* be that, in these regimes, Population 1 should be the stronger of the two populations, i.e. the steady-state solutions will give $0 \leq \bar{P}_2 < 0.5 < \bar{P}_1 \leq 1$. However, in Cases Y and Z, Population 2 is able to downregulate Population 1 ($0 \leq \bar{P}_1 < 0.5 < \bar{P}_2 \leq 1$) if subject to suitable initial conditions.

which arises. When we do depart from (38), (42) or (52), the initial conditions adopted will be described in the caption of the relevant figure. Time dependent numerical solutions are calculated using the ode15s solver in MATLAB v7.1 (The MathWorks, Inc.) and steady-state solutions are computed in XPPAUT 5.91; all plots were created in MATLAB v7.1.

3.2 Relative population size, N

3.2.1 Model I

$N = 1$ implies that the populations are of equal size (and large by assumption) and the populations behave identically (both quickly achieve an up-regulated state, see Figure 4). Increasing $N = N_1/N_2$ is equivalent to making Population 1 larger than Population 2 (more specifically, since N_1 appears in the definition of other nondimensional parameters that remain fixed, increasing N corresponds to decreasing the size of Population 2). We expect that for N sufficiently large, Population 2 will be forced into a down-regulated state ($\bar{P}_2 < 0.5$) as a result of competitive QS, allowing Population 1 to dominate ($\bar{P}_1$ is close to 1), i.e. Case W. Figures 4(a) (time-dependent dynamics) and (b) (bifurcation diagram) show that this does indeed occur. For $N = 1$, both groups reach an up-regulated state (Case V) since both groups are equal and large in size, but as we increase N, the first population begins to dominate, and two fold bifurcations emerge giving Case X (this structure being familiar from the single strain models [26, 27, 30]). For $N \gtrsim 2.5$, the second population can either become active or be suppressed into an inactive state. When N is large enough, the second population is necessarily inactivated (Case W). Throughout the range $N > 1$, Population 1 remains in an active state. Thus, for $N > 1$ either both populations will finish in an active state or Population 1 will downregulate Population 2. For $N < 1$, we have the equivalent behaviour in reverse, i.e. for sufficiently small N, Population 2 inactivates Population 1 (data not shown). The unstable steady state separating the two stable steady states can be viewed as a border line between them: we can expect that initial conditions lying between the unstable steady state and the up-regulated stable state will allow Population 2 (within the bistable region of $N > 1$) to become active (i.e. $\bar{P}_2 > 0.5$).
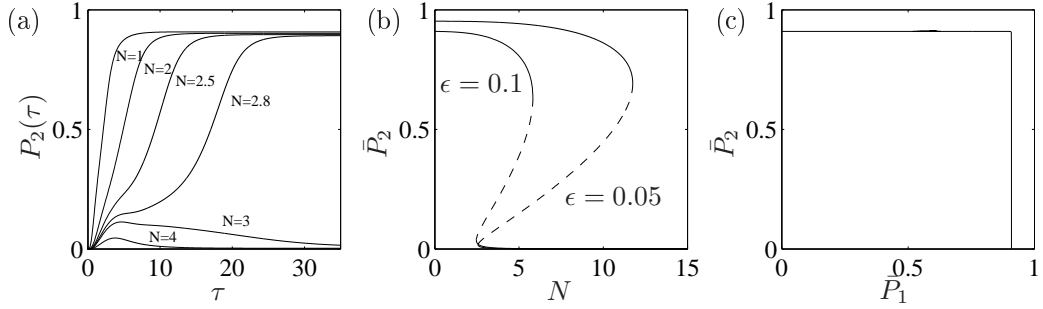
Figure 4: (a) Dynamics of P_2 in Model I for various N with $\epsilon = 0.1$ (remember that τ represents nondimensional time, see (15)). The dramatic decrease in Population 2's regulation level suggests a bifurcation, and bifurcations in fact occur at both $N \approx 2.47$ and $N \approx 5.82$ (see (b)). The corresponding curves for P_1 all reach an up-regulated state and are not easily distinguishable from that shown here for $N = 1$. (b) Steady-state solutions for P_2 (i.e., $\bar{P}_2$) in Model I with bifurcation parameter N. Smaller ϵ implies that the difference between basal transcription and QS-induced transcription is more pronounced, i.e. the switch between down- and up-regulated states should occur faster and be more rigid. In (c) we plot the projection of the bifurcation curve onto the $\bar{P}_1 - \bar{P}_2$ plane when $\epsilon = 0.1$.

3.2.2 Model II

Model II results in slightly different behaviour around $N = 1$; Figure 5 shows the bifurcation diagrams for $\bar{P}_1$ and $\bar{P}_2$ (these being the P_1 and P_2 components of the steady state respectively) as we vary N. For this model there exists an interval around $N = 1$ in which three stable steady states exist (Case Z): either both populations are up-regulated, or either population can downregulate the other; separating each of these is an unstable steady state. The unstable steady states thus delineate a population's ability to fend off the opposition AIP. If N is increased outside of the tristable interval, the system becomes bistable and, if increased further, monostable. In the bistable region, either population can inactivate the other (Case Y) and in the monostable region, Population 1 necessarily downregulates Population 2 giving Case W (the equivalent but opposite behaviours occur for decreasing N). The behaviour differs from Model I, which has two bistable regimes (one in $N < 1$ and the other in $N > 1$). In Model II these regimes essentially merge, overlapping around $N = 1$ and forming a tristable region. We saw in [26] that the Model II TCS is the most sensitive of the three TCSs to inhibition and this is further evidence that this is the case for our parameter choice: if Population 2 begins in a more
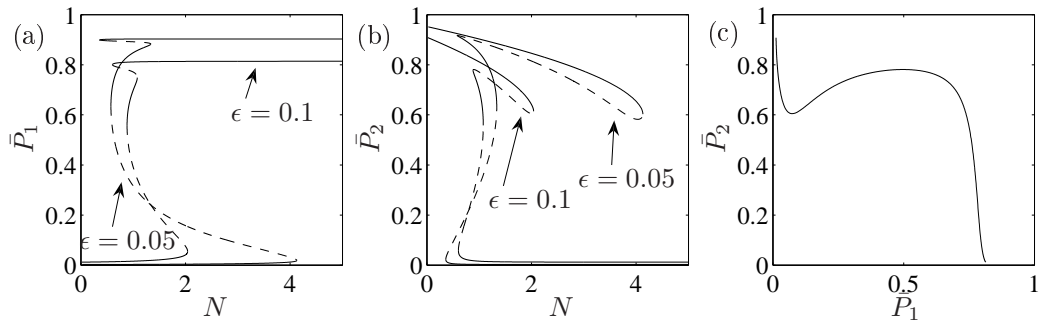
Figure 5: Bifurcation diagrams for (a) $\bar{P}_1$ and (b) $\bar{P}_2$ in Model II for $\epsilon = 0.1$ and $\epsilon = 0.05$. In (c) we plot the projection of the bifurcation curve onto the $\bar{P}_1 - \bar{P}_2$ plane when $\epsilon = 0.1$. This model displays noteworthy behaviour for N close to unity, where a tristable region exists (Case Z). Outside of the tristable region the system becomes bistable and then monostable where in the latter case, for $N > 1$ Population 1 necessarily inactivates Population 2 and vice versa for $N < 1$.

agr-active state than Population 1 (i.e. $P_2(0) > P_1(0)$) then it may be of no consequence that Population 1 is the larger population (within the multistable region only), and Population 2 can overcome Population 1 (i.e. $1 \geq \bar{P}_2 > 0.5 > \bar{P}_1 \geq 0$) simply by having more cells active initially. Thus the sensitivity of this particular TCS to inhibition here results in the initial conditions of the system being potentially more influential than the relative population sizes (again, within the multistable region only) because the Population 1 cells can be inhibited quickly by the already active Population 2 cells.

3.2.3 Model III

Qualitatively, Model III behaves in much the same way as Model I: see Figure 6. As with Model I, we have Cases V, W and X (the last of these representing the bistable regime); thus over the whole range $N > 1$, either both populations achieve an up-regulated state (for sufficiently small $N > 1$) or Population 1 inactivates Population 2 (for sufficiently large $N > 1$). For $N < 1$, a similar bistable regime occurs which gives the converse behaviour. Note that with $\epsilon = 0.1$, Population 1 only needs to be around 2.2 times the size of its counterpart to guarantee success, compared with approximately 5.82 times in Model I and 2.04 times for Model II; this is consistent with the relative efficiency of the three TCS cascades to withstand inhibitor therapy demonstrated in [26], i.e. Model I is the most robust to inhibition and Model II the most sensitive.
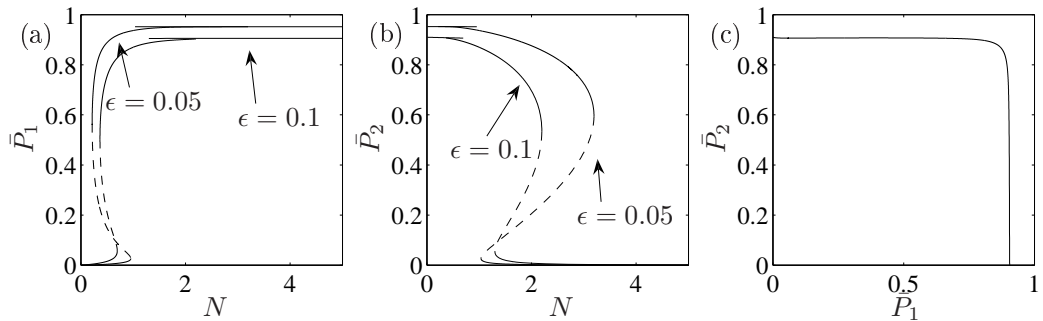
Figure 6: Solution curves for (a) $\bar{P}_1$ and (b) $\bar{P}_2$ in Model III for $\epsilon = 0.1$ and $\epsilon = 0.05$. These numerical results match the behaviour which would be anticipated biologically: the larger population is able to downregulate its counterpart. Each curve contains four fold bifurcations: two for $N < 1$ (clearest on the $\bar{P}_1$ curves) and two for $N > 1$ (clearest on the $\bar{P}_2$ curves). In (c) we plot the projection of the bifurcation curve onto the $\bar{P}_1 - \bar{P}_2$ plane when $\epsilon = 0.1$.

It is evident that decreasing ϵ increases the range of N over which multi-stability exists for each model; numerical investigations indicate that this is the case also for the remaining analyses performed in this study. Henceforth, we display only the $\epsilon = 0.1$ solutions.

3.3 Relative self-activating binding rate, β_A

3.3.1 Model I

We examine how altering the potency of the different AIPs affects the regulation of their respective populations. Figure 7 shows the solution curve of P_2 of Model I with bifurcation parameter β_A. Since we fix β_{11} (the rate of self-activating binding in Population 1), increasing $1/\beta_A$ (the ratio of the rate of self-activating binding in Population 1 to that of Population 2) is equivalent to increasing the difference between the self-activating potencies of the two populations' AIPs, so that $1/\beta_A > 1$ means Population 1 has a faster self-activating binding rate than Population 2. We see that increasing $1/\beta_A$ yields cases V, W and X once again as the first population is able to push the second into downregulation, as would be expected.

3.3.2 Model II

As in §3.2, Model II produces different behaviour to Model I, this time for varying β_A - see Figure 8. We now
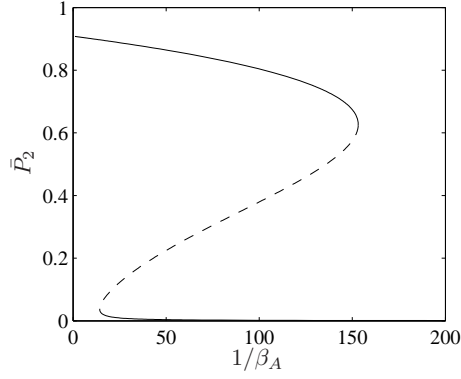
23

Figure 7: Bifurcation diagram for $\bar{P}_2$ against $1/\beta_A$ for Model I. Increasing $1/\beta_A$ is equivalent to Population 1 AIP binding 1
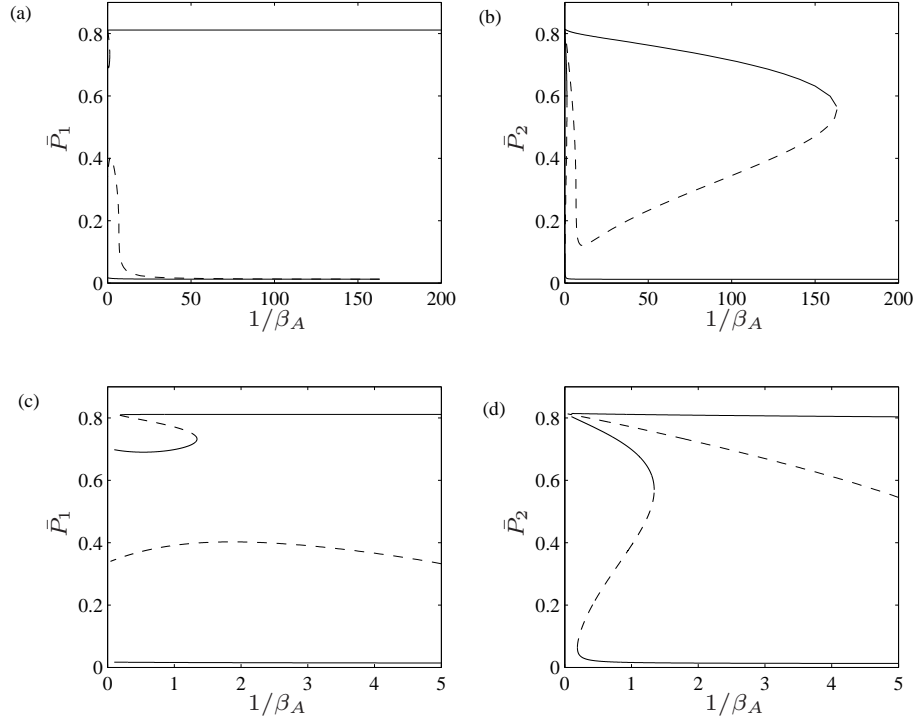

Figure 8: Bifurcation diagrams for (a) $\bar{P}_1$ and (b) $\bar{P}_2$ with the nondimensional parameter β_A, in Model II. In (c) and (d) the diagrams are focused on the lower range of $1/\beta_A$ to be able to see clearly the behaviour of the system here. In addition to the hysteretic curve seen in previous diagrams, an additional solution curve exists yielding unexpected behaviour from the system (Cases Y and Z): there exists a regime where either population can downregulate the other. Though it is not clear from (d), the two solution curves for $\bar{P}_2$ (i.e. the lower two-fold curve and the higher single-fold curve) do not meet.

have two solution curves: the usual pair of fold bifurcations and an extra curve which behaves in a more unusual fashion. For sufficiently large $1/\beta_A$ (roughly $1/\beta_A > 164$ for $\epsilon = 0.1$), Case W arises whereby Population 1 necessarily inactivates Population 2. For $1 < 1/\beta_A < 163$ (with $\epsilon = 0.1$), Cases Y and Z occur, meaning that, depending upon the initial conditions, either population could downregulate the other. Given that in this interval Population 1 has a higher self-activation rate than Population 2, the possibility that Population 2 could inactivate Population 1 could be deemed to be somewhat surprising (we would ordinarily anticipate that this would occur for $1/\beta_A < 1$).

In Figure 9, we present a time-dependent solution illustrating how Population 2 could achieve domination when $\beta_A = 1/20$ (i.e. from the bistable Case Y and when Population 1 has the faster rate of self-activation). Population 2's initial level of activity ($P_2(0)$) is taken to be higher than that of Population 1 ($P_1(0)$). The first population initially binds to its AIP so quickly that not enough of its AIP reaches the second population, resulting in a higher concentration of free receptors in the second population (see R_j). Because this population begins in a more active state, it can manipulate this situation to build up a bigger AIP supply (see a_j) with which it can not only activate itself but also inhibit the opposition (see P_j). We note that our numerical investigations suggest that it is a requirement that Population 2 begin in a more active state (or at least not significantly lower) than Population 1 ($P_2(0) > P_1(0)$) for it to dominate ($\bar{P}_2 > \bar{P}_1$) in this parameter regime, implying that having a faster self-activation rate resulting in AIP being wasted on cognate cells (leaving insufficient amount to downregulate the opposition cells) is not the sole reason for Population 2 dominating: fewer Population 1 cells must also be active initially.

3.3.3 Model III

Figure 10 illustrates the solution curves for varying β_A in Model III. As for Model II, there is an additional branch of solutions which enables the 'weaker' population (that with the slower rate of self-activation) to dominate, giving Cases V, W, X and Y. Notice that here both of the 'usual' fold bifurcations occur for $1/\beta_A > 1$ (meaning that Case V also arises for Model III), while for Model II they lie either side of $\beta_A = 1$. This again illustrates the higher sensitivity of Model II to inhibition compared to Models I and III for our parameter choice: for Model II the difference between the two populations needs to be less pronounced than for either Model I or Model III in order to ensure that one population is dominant.
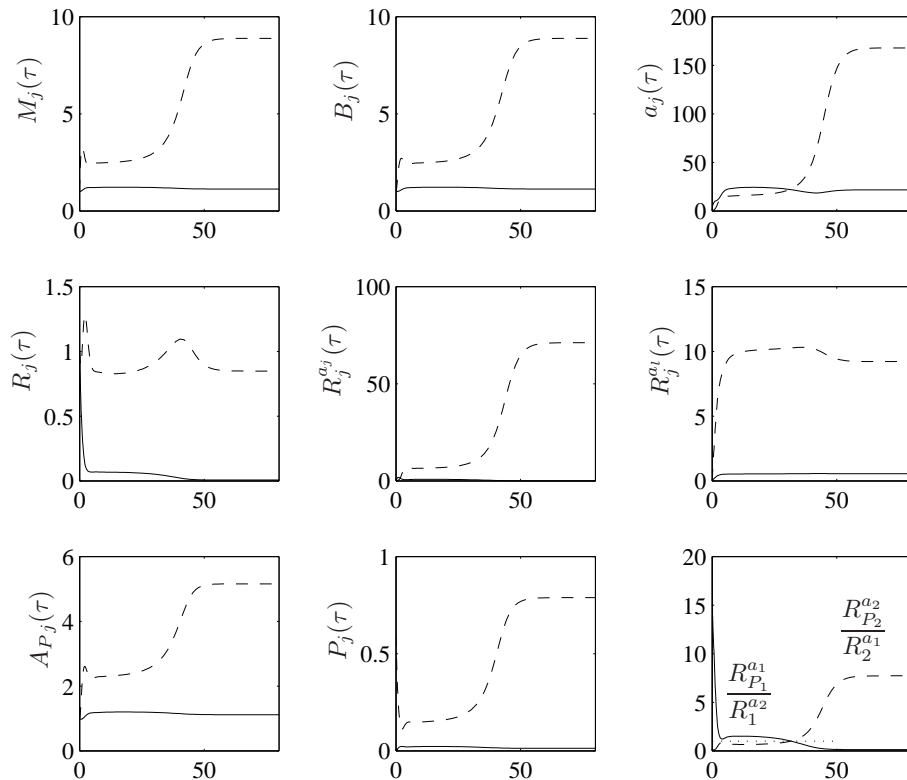
Figure 9: Time-dependent numerical solution to Model II (equations (22), (24)-(35) and (39)-(41)) for a selection of variables with $1/\beta_A = 20$, all other parameters from Table 3(a) and the only altered initial condition from (38) and (42) being $P_2(0) = 0.6$ and $P_1(0) = 0$. The solid lines represent Population 1 variables ($j = 1, l = 2$) and dashed lines those of Population 2 ($j = 2, l = 1$). Population 2 manipulates the advantage it has through a higher initial level of activity than Population 1 to inactivate the latter. In the final graph we depict the ratio of self-bound receptors to opposition-bound receptors for each population, i.e. the solid line describes $R_{P_1}{}^{a_1}/R_1{}^{a_2}$ and the dashed line $R_{P_2}{}^{a_2}/R_2{}^{a_1}$ (the dotted line simply corresponds to a ratio of one), concisely demonstrating the switch in control of the two populations.
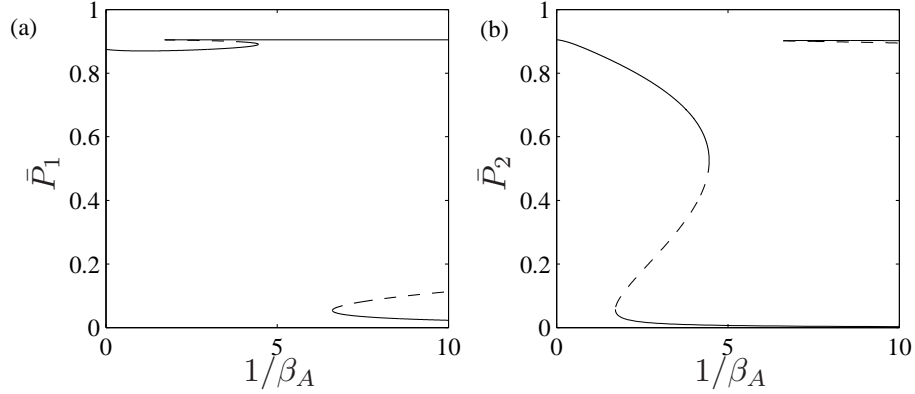
Figure 10: Steady-state curves for (a) $\bar{P}_1$ and (b) $\bar{P}_2$ of Model III as $1/\beta_A$ varies. Cases V, W, X and Y are all possible.

Figure 11 provides an example of the time-dependent dynamics in Case Y (where either population can inactivate the other) though, in contrast to Figure 9, we illustrate a solution where Population 1 uses the advantage of a faster rate of self-activation to overcome the disadvantage of having 'weaker' initial conditions $(P_1(0) < P_2(0))$.

3.4 Relative cross-inhibition binding rate, β_I

3.4.1 Model I

So far, all results for Model I have been in accordance with intuition. However, altering β_I (the ratio of the rate of inhibitory binding in Population 1 to that of Population 2) produces a more surprising result. Not only do we see the hysteretic curve familiar from §3.2.1 and §3.3.1 as we increase β_I (equivalent to making the first population's inhibiting ability more potent relative to the second's), but we also see the emergence of two new steady states, one stable and one unstable; see Figure 12. Consequently Cases V, X, Y and Z arise for Model I when β_I is the bifurcation parameter. Although each of these cases means Population 1 can (with suitable initial conditions) downregulate Population 2, it can never be guaranteed and the last two allow for the possibility that Population 1 will be inactivated by Population 2 despite having a greater inhibitory binding rate. In order to gain some insight into why this is possible, some numerical solutions are provided in the appendix with $\beta_I = 180$ (which gives Case Y: either population can inactivate the other); see Figures
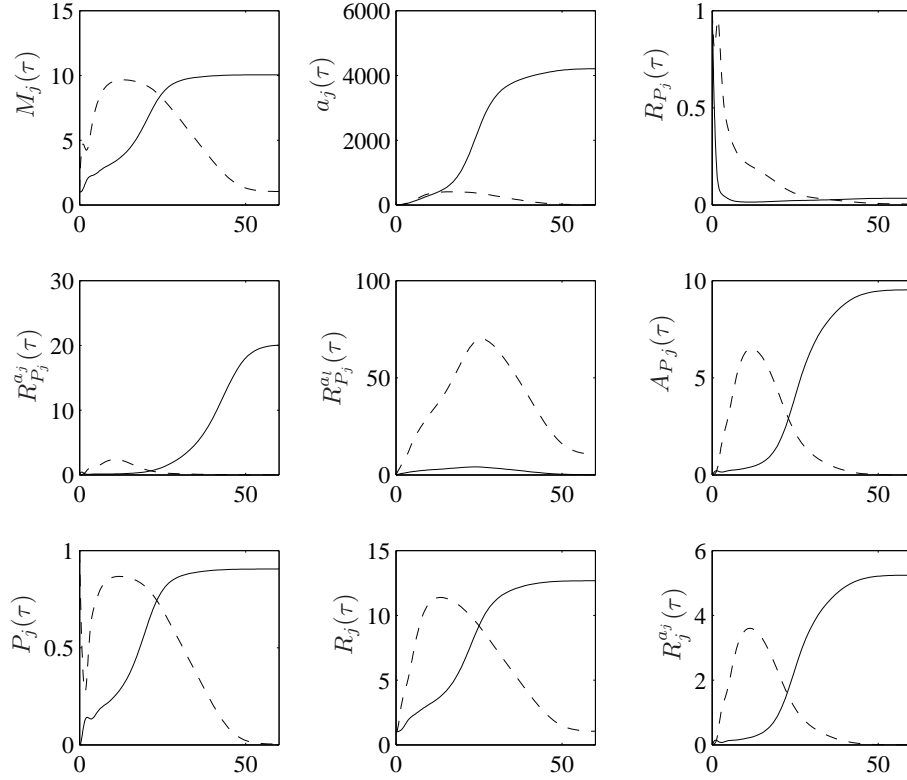
Figure 11: Time-dependent numerical solution for a selection of variables of Model III (solid lines: Population 1, dashed lines: Population 2) with $1/\beta_A = 10$ (the bistable Case Y where either population can downregulate the other), all other parameters from Table 3(a) and initial conditions (38) and (52) for all variables except P_2, for which $P_2(0) = 1$. The solutions tend initially toward Population 2 achieving upregulation; the advantage held by Population 1 by having a faster self-activating binding rate enables Population 1 to ultimately become active despite Population 2 beginning with the maximum value of $P_2(0)$, downregulating Population 2 in the process.
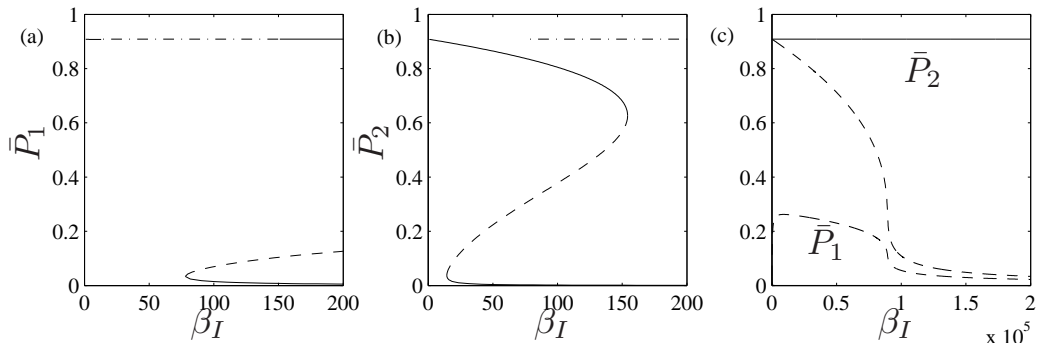
Figure 12: Bifurcation diagrams for (a) $\bar{P}_1$ and (b) $\bar{P}_2$ with bifurcation parameter β_I for Model I. Cases V, X, Y and Z are all possible. The three branches of the hysteretic curve in (a) are indistinguishable on this scale and so are illustrated with the dot-dash line; the same applies to the two branches of the single-fold curve in (b). In order to be able to see the shape of this single-fold curve, it is plotted for both $\bar{P}_1$ and $\bar{P}_2$ in (c).

20-22 and the accompanying discussion. In each figure we use different initial conditions in order to allow the model to evolve to either of the possible stable steady states depicted in the bifurcation diagram of Figure 12 for $\beta_I = 180$.

The extra single-fold solution curve (which makes Cases Y and Z possible) suggests that the cells could in some sense be too efficient for their own good at fighting off other species: producing an AIP which is too potent can be detrimental to their own efforts at becoming the dominant species.

Whilst mathematically interesting, we must bear in mind whether a realistic parameter choice would allow Cases Y and Z to exist. Since we have taken $\beta_{11} = \beta_{21} = O(1/\epsilon)$ in Figure 12 (where $\epsilon = 0.1$), the majority of the parameter range illustrated by these bifurcation diagrams has the dimensional β_{12} far greater than the dimensional β_{11}, meaning that an AIP's ability to bind to opposing strains is greater than its ability to bind to its own strain which would seem somewhat unlikely. In the more biologically realistic regime where this is not the case, both populations simply reach an active state, rendering much of the previous discussion in this section relevant only if engineering a strain for therapeutic purposes, in which case the signal molecule structure could be specified, and therefore, to a certain extent, its binding ability also.

A more biologically realistic investigation into what happens for varying β_I, perhaps, is to set the self-activating binding rate to be *larger* than the inhibiting binding rates. Such an investigation (performed numer-
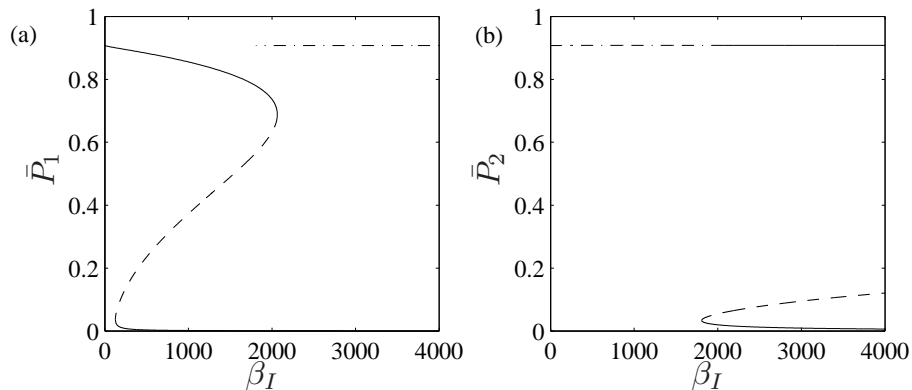
29

Figure 13: Bifurcation diagrams for (a) $\bar{P}_1$ and (b) $\bar{P}_2$ of Model I with varying β_I when $\beta_{11} = 100$ (all other parameters are taken from Table 3(a)). The dot-dash lines again represent multiple branches which are indistinguishable from each other. In (a) the dot-dash line is the single-fold branch and in (b) it encompasses the bistable hysteretic curve.

ically, but results not shown) shows that qualitatively the same bifurcation curves are produced for any value of β_{11} with $10 \le \beta_{11} \le 50$ (when $\epsilon = 0.1$). However, for $\beta_{11} > 50$ there is a switch in the behaviour of the two populations: the bifurcation diagram for P_1 now resembles that of P_2 for $10 \le \beta_{11} \le 50$ and P_2 that of P_1, i.e Cases V, X, Y and Z all still exist but the roles of the two populations are reversed in all of these, see Figure 13. However, this is, again, likely to be irrelevant in practice: the area of the graph where Population 1's inhibiting rate is slower or equal to its activating rate corresponds to $\beta_I \le 10$ where both populations are up-regulated, i.e. if the self-activating abilities are sufficiently high then altering the inhibiting ability has little effect: both populations will still be in a position to upregulate themselves. This switch in roles also occurs for Model III and we discuss this further in §3.4.3.

Interestingly, if $N > 1$ Case Z is no longer possible with varying β_I and Case Y occurs only in an unrealistic domain of β_I (once $N > 8$, Case Y exists only for $\beta_I >> 10^4$), while the more intuitive Cases V, X and W (these cover both populations achieving upregulation or Population 1 inactivating Population 2) exist for much more plausible values of β_I, see Figure 14. If N is sufficiently large, the dimensional β_{12} does not even need to be larger than the dimensional β_{21} to guarantee that the first population will downregulate the second (Case W), i.e. population size is more influential in determining the outcome than the relative binding abilities.
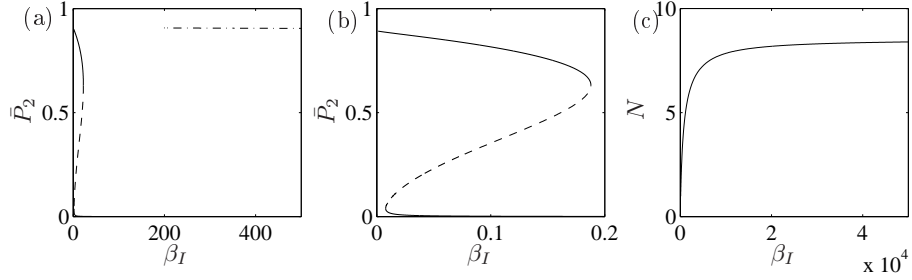
30

Figure 14: Bifurcation diagrams for $\bar{P}_2$ when (a) $N = 2$ and (b) $N = 10$ in Model I with varying β_I (and all other parameters taken from Table 3(a)). In (a) the dot-dash line comprises the stable and unstable branches of the single-fold curve. In (c) we depict the dependence on N of the minimum value of β_I at which Case Y (either population can downregulate the other) arises. For values of β_I lower than those tracked here, either both populations reach an active state or Population 1 inactivates Population 2. In (b) the minimum value at which Case Y can arise (i.e., the turning point of the single-fold curve) occurs at $\beta_I > 5 \times 10^4$, see (c); we do not illustrate this solution curve here.

3.4.2 Model II

We obtain similar bifurcation curves, see Figure 15, as for Model I in §3.4.1. The main difference is that only the tristable Case Z and bistable Case Y exist for Model II, i.e. given suitable initial conditions, either population can downregulate the other regardless of β_I. Consequently, this behaviour exists in a potentially realistic parameter range (where inhibiting binding rates do not differ greatly from self-activation rates) for Model II.

3.4.3 Model III

Model III is qualitatively similar to Models I and II for varying β_I, see Figure 16. Quantitatively the corresponding fold bifurcations lie at values of β_I between those of the previous two models (meaning the possible cases are different for Model III), again reflecting the results of [26] which demonstrated that the Model III TCS would be middle of the three in terms of sensitivity to inhibitor therapy.

As for Model I, Case Y (where Population 2 can downregulate Population 1 despite having a lower inhibiting binding ability) occurs only in a range of β_I that is unlikely to be biologically relevant (where the inhibitory
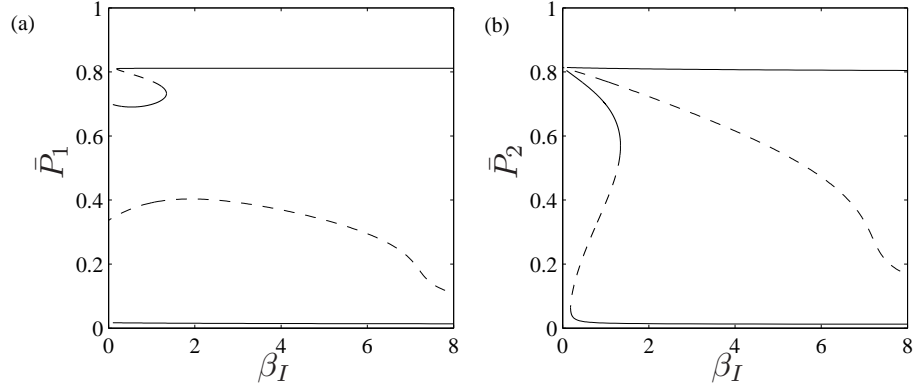
31

Figure 15: Bifurcation diagrams for (a) $\bar{P}_1$ and (b) $\bar{P}_2$ of Model II as β_I is varied with all other parameters taken from Table 3(a). This behaviour is qualitatively similar to that of Model I but, for Model II, all of the fold bifurcations occur at much lower values of β_I (compare with Figure 12).
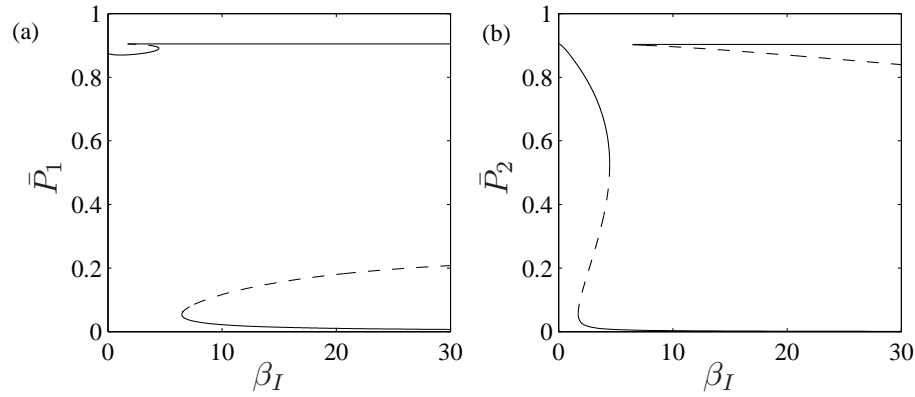

Figure 16: The steady-state curves for (a) $\bar{P}_1$ and (b) $\bar{P}_2$ of Model III as functions of β_I, with all other parameters taken from Table 3(a). As for Model II in Figure 15, the behaviour of Model III with respect to β_I is qualitatively similar to that of Model I, but the fold bifurcations occur at lower values of β_I (though at higher values than Model II).
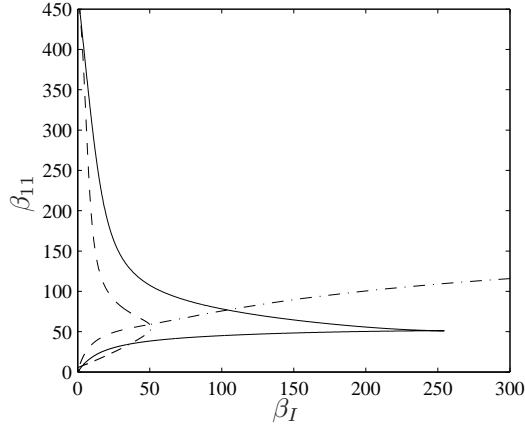
Figure 17: As β_I varies in Model III, two possible solution curves exist: a hysteretic curve and a single-fold curve, see Figures 16 and 18. The values of β_I at which these fold locations lie are dependent upon β_{11} and we here demonstrate these locations. The dot-dash curve illustrates the location of the fold on the single-fold curve (the minimum value of β_I at which Case Y arises), the dashed curve that of the lower fold (by this we mean lower in terms of the value of β_I at which it occurs, rather than the value of $\bar{P}_1$ or $\bar{P}_2$) of the hysteretic curve (the minimum value at which Case X can occur) and, finally, the solid curve its upper fold (similarly, the upper fold corresponds to the fold on the hysteretic curve which occurs at the larger value of β_I), the minimum value of β_I giving Case W. Where the dot-dash and dashed curves meet, the roles of the two populations in Cases W, X and Y are reversed.
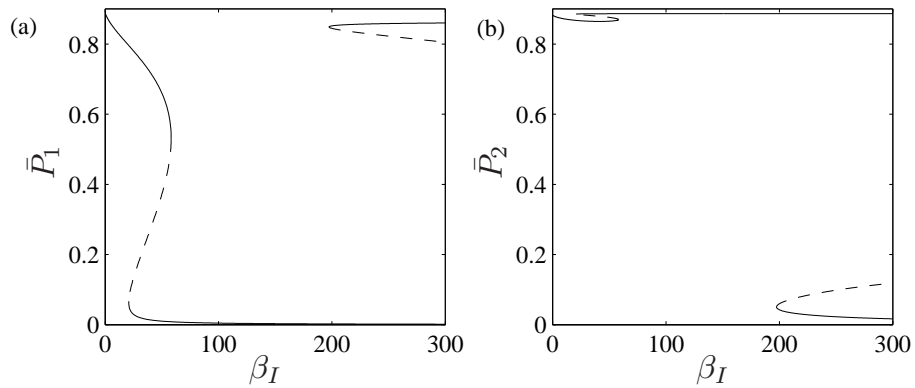

Figure 18: Bifurcation diagrams for (a) P_1 and (b) P_2 for Model III as functions of β_I for $\beta_{11} = 100$, with all other parameters taken from Table 3(a). The larger value of β_{11} employed here (rather than in Figure 16) switches the roles of the two populations from Figure 16 in each of the Cases V, W, X and Y.

33

binding rate is greater than the activating rate), meaning that only Cases V, W and X (where either both populations are active or Population 1 downregulates Population 2) are potentially realistic; in Figure 17 the boundaries of each case are illustrated. Similarly to Model I, increasing β_{11} (the self-activating binding rate) by a sufficient amount produces a switch in the behaviour of the two populations: taking β_{11} large enough results in the roles of each population in each case (Cases V, W, X, Y) being reversed from their roles for smaller β_{11} (Figure 18 illustrates this when $\beta_{11} = 100$). If both populations have a sufficiently large self-activating binding rate (i.e. large β_{11}), then providing Population 1 with quicker inhibitory binding than Population 2 is beneficial only to the latter, i.e. if the cells can bind to their own AIP sufficiently quickly then they are better off with slower inhibitory binding, else they risk being suppressed by the opposition cells. In terms of our model, by losing some AIP to the opposition cells, Population 1 is at a disadvantage since Population 2 will upregulate itself regardless (given the fact that it has a large self-activating binding rate). While Population 1 also has this fast rate, it will lose enough AIP to the opposition bacteria to make itself the weaker population. In other words, in this scenario it is important to reach an active state before attempting to downregulate the opposition bacteria - see Figure 19.

4   Discussion

The *agr* system is employed by many Gram-positive bacteria, including a number of important pathogens. It has been demonstrated that *S. aureus* uses the *agr* operon as a means of communication, with strains able to activate the *agr* operon of strains from within the same group and inhibit that of other groups. This cross-strain antagonism has therapeutic implications: a non-pathogenic, inhibitory AIP producing strain of *S. aureus* could be designed to be administered at the site of a staphylococcal infection in order to inhibit the *agr* system of the infecting strain, inactivating the production of certain virulence factors and allowing the host's immune system an increased chance of eliminating the pathogen.

We have investigated the effect of altering certain aspects of the cells in this process by analysing their steady-state behaviour. The stable steady states determine the ultimate outcome of the systems, while the unstable ones are influential in determining the basins of attraction of the stable states. For example, when there are two stable steady states for a given parameter set, where one has Population 1 suppressing Population 2, and
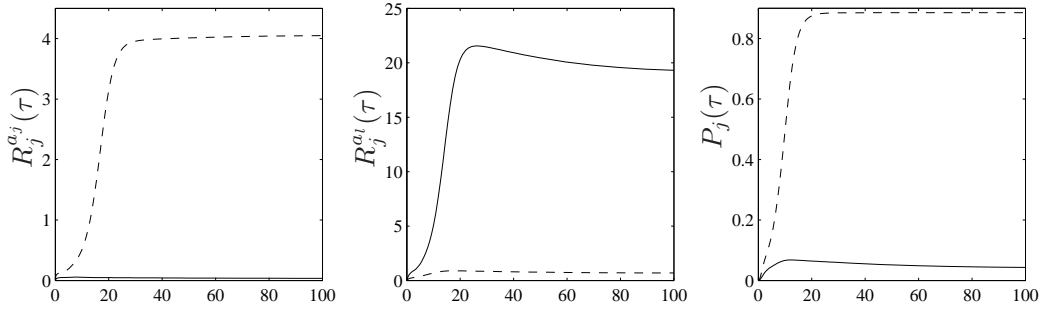
Figure 19: Time-dependent numerical solution to Model III using the default initial conditions, $\beta_{11} = 100$, $\beta_I = 22$ (i.e. in the regime where either both populations will become active or Population 2 will suppress Population 1) and all other parameters from Table 3(a) ($j = 1, 2$ and $l = 3 - j$). Although Population 1 (solid line) has a higher inhibiting binding rate than Population 2 (dashed line), as both populations have a high self-activating binding rate (i.e. because $\beta_{11} = 100$), the second population will activate itself quicker since the first will lose more of its own AIP through its attempt at inactivating the opposition cells than vice versa; the second population is consequently in a better position to suppress the QS systems of the first. This demonstrates the importance of reaching an active state as quickly as possible: the second population has already begun the process of upregulation before the first population's AIP has made any real progress in binding to the opposition cells.

the other vice versa, the unstable steady state lying between them can be seen to represent both populations attempting to inactivate each other, but the initial conditions of the system will ultimately determine to which stable state the model is drawn. We considered the effects of varying three factors of the two populations, namely their relative sizes, self-activation potencies and inhibitory potencies. If one population is larger or has faster self-activating or inhibiting rates than the other then there exists the possibility that it will downregulate the second strain; however, this could not always be guaranteed. In many situations, the opposite behaviour to what might be anticipated was also possible (Cases Y and Z) and sometimes even when the initial conditions of the populations were identical. We modelled the three different possible cascades of the TCS and in the case of the classical TCS (Model I) we showed that Cases Y and Z arose only in a potentially unrealistic parameter range. In Models II and III (representing alternative TCS cascades), on the other hand, such behaviour *could* appear in a realistic parameter range.

The mechanistic details of the *agr* system can lead to significant differences in the behaviour of competing strains and the differences between the models provide plausible approaches to assessing which cascade is in operation in the TCS of the *agr* operon of a given strain (either of *S. aureus* or other Gram-positive bacteria). For instance, if the unexpected behaviour as outlined by Cases Y and Z is impossible to reproduce experimentally then this is an indication that a classical TCS governs the *agr* operon.

The results for Model II are less clear cut than for the other two systems: for each parameter variation, there was a tristable region around the parameter value which corresponded to the populations having equal 'strength' where either both populations were up-regulated or one dominated over the other; the parameters had to be increased or decreased sufficiently away from 1 to lose this tristable behaviour. Thus the Model II TCS (where AgrA is constitutively phosphorylated) is weaker than the remaining two TCSs in terms of fending off inhibition, with the Model I TCS (the classical TCS) being the most robust. This is also a reflection of the TCS in isolation and not simply as part of the overall signalling system and these results, therefore, are likely to transfer to other operons beyond the *agr* system and to bacteria employing similar signal transduction systems.

Furthermore, if a TCS cascade has been fully characterised for a specific strain or species, these investigations provide pointers regarding the use of QS for therapeutic purposes which could be investigated experimentally in animal infection models after engineering a specific cross-group inhibitory AIP into a non-pathogenic strain.

For instance, the analyses provide indications on the features and quantities required of a therapeutic strain to ensure that the infecting strain will be down-regulated. The only parameter that guarantees for all three models that the behaviour is as might naively be expected if made sufficiently large or small is N, the ratio of the population sizes, confirming the intuition that this is the key to ensuring therapeutic success through interference with the QS system. On the other hand, the relative rate of inhibitory binding was the least robust of the three parameters studied in terms of outcome and therefore likely to prove a much more precarious target for a 'designer' strain. Concentrating solely on the relative population sizes, however, may not always be wise: administering a sufficiently large population of bacteria (albeit non-pathogenic) to an infection site would not always be practical. In such circumstances, the analyses presented in this work can be drawn upon to guide the design of a strain which is effective with a more feasible population size, for example by carefully specifying the self-activating rate of the new strain. This analysis, therefore, provides early guidance in the development of such a therapy; many more factors (such as the effect of cell growth rate upon the dynamics of the system or the potential persistence of an *agr* down-regulated infecting strain due to increased colonisation factor production) must also be considered. Furthermore, it will be necessary to consider the consequences of two competing strains utilising different phosphorelays in their TCSs (in this study we have concentrated solely upon the scenario where competing strains employ identical phosphorelays).

QS is not restricted to pathogenesis in bacteria. It is an important cell communication system which is already known to serve a variety of purposes in an increasing number of bacteria and the likelihood is that, as the study of QS systems continues, numerous other functions will be discovered. Many of these will be of interest due to the benefits which they can bestow, rather than because of the harm which they can cause. For instance, the discovery of the *agr* operon in the clostridial species [12, 13, 31] may yield a link between QS and the production of biofuels by bacteria such as *Clostridium acetobutylicum* which can be exploited for environmental and economic gain. Analyses such as those presented here (though focusing on mutually activating systems which could cause the premature upregulation of a particular strain rather than its inactivation) should therefore assist in the acceleration of such processes.

Acknowledgements

References

[1] Nealson K.H., Hastings J.W. (1979) Bacterial bioluminescence: its control and ecological significance. *Microbiol. Rev.,* 43, 496–518.

[2] Williams P., Winzer K., Chan W.C., Cámara M. (2007) Look who's talking: communication and quorum sensing in the bacterial world. *Philos. T. Roy. Soc. B,* 362, 1119–1134.

[3] Atkinson S., Williams P. (2009) Quorum sensing and social networking in the microbial world. *J. Roy. Soc. Interface,* 6, 959–978.

[4] Salmond G.P.C., Bycroft B.W., Stewart G.S.A.B., Williams P. (1995) The bacterial 'enigma': cracking the code of cell-cell communication. *Mol. Microbiol.,* 16, 615–624.

[5] Riedel K., Hentzer M., Geisenberger O., Huber B., Steidle A., Wu H., Hœiby N., Givskov M., Molin S., Eberl L. (2001) N-Aclyhomoserine-lactone-mediated communication between *Pseudomonas aeruginosa* and *Burkholderia cepacia* in mixed biofilms. *Microbiology,* 147, 3249–3262.

[6] Qazi S., Middleton B., Muharram S.H., Cockayne A., Hill P., O'Shea P., Chhabra S.R., Cámara M., Williams P. (2006) N-Acylhomoserine lactones antagonize virulence gene expression and quorum sensing in *Staphylococcus aureus*. *Infect. Immun.,* 74, 910–919.

[7] Ji G., Beavis R., Novick R.P. (1997) Bacterial interference caused by autoinducing peptide variants. *Science,* 276, 2027–2030.

[8] Otto M., Süßmuth R., Vuong C., Jung G., Götz F. (1999) Inhibition of virulence factor expression in *Staphylococcus aureus* by the *Staphylococcus epidermidis agr* pheromone and derivatives. *FEBS Lett.,* 450, 257–262.

[9] Otto M., Echner H., Voelter W., Götz F. (2001) Pheromone cross-inhibition between *Staphylococcus aureus* and *Staphylococcus epidermidis*. *Infect. Immun.,* 69, 1957–1960.

[10] McDowell P., Affas Z., Reynolds C., Holden M.T.G., Wood S.J., Saint S., Cockayne A., Hill P.J., Dodd C.E.R., Bycroft B.W., Chan W.C., Williams P. (2001) Structure, activity and evolution of the group I thiolactone peptide quorum-sensing system of *Staphylococcus aureus*. *Mol. Microbiol.,* 41, 503–512.

[11] Novick R.P. (2003) Autoinduction and signal transduction in the regulation of staphylococcal virulence. *Mol. Microbiol.,* 48, 1429–1449.

[12] Sebaihia M., Peck M.W., Minton N.P. *et al.* (2007) Genome sequence of a proteolytic (Group I) *Clostridium botulinum* strain Hall A and comparative analysis of the clostridial genomes. *Genome Res.,* 17, 1082–1092.

[13] Ohtani K., Yuan Y., Hassan S., Wang R., Wang Y., Shimizu T. (2009) Virulence gene regulation by the *agr* system in *Clostridium perfringens*. *J. Bacteriol.,* 191, 3919–3927.

[14] Podbielski A., Kreikemeyer B. (2004) Cell density-dependent regulation: basic principles and effects on the virulence of Gram-positive cocci. *Int. J. Infect. Dis.,* 8, 81–95.

[15] Riedel C.U., Monk I.R., Casey P.G., Waidmann M.S., Gahan C.G.M., Hill C. (2009) AgrD-dependent quorum sensing affects biofilm formation, invasion, virulence and global gene expression profiles in *Listeria monocytogenes*. *Mol. Microbiol.,* 71, 1177–1189.

[16] Novick R.P., Ross H.F., Projan S.J., Kornblum J., Kreiswirth B., Moghazeh S. (1993) Synthesis of staphylococcal virulence factors is controlled by a regulatory RNA molecule. *EMBO J.,* 12, 3967–3975.

[17] Zhang L., Gray L., Novick R.P., Ji G. (2002) Transmembrane topology of AgrB, the protein involved in the post-translational modification of AgrD in *Staphylococcus aureus*. *J. Biol. Chem.,* 277, 34736–34742.

[18] Zhang L., Lin J., Ji G. (2004) Membrane anchoring of the AgrD N-terminal amphipathic region is required for its processing to produce a quorum-sensing pheromone in *Staphylococcus aureus*. *J. Biol. Chem.,* 279, 19448–19456.

[19] Queck S.Y., Jameson-Lee M., Villaruz A.E., Bach T.H.L., Khan B.A., Sturdevant D.E., Ricklefs S.M., Li M., Otto M. (2008) RNAIII-independent target gene control by the *agr* quorum-sensing system: insight into the evolution of virulence regulation in *Staphylococcus aureus*. *Mol. Cell,* 32, 150–158.

[20] Cisar E.A.G., Geisinger E., Muir T.W., Novick R.P. (2009) Symmetric signalling within asymmetric dimers of the *Staphylococcus aureus* receptor histidine kinase AgrC. *Mol. Microbiol.,* 74, 44–57.

[21] Stock A.M., Robinson V.L., Goudreau P.N. (2000) Two-component signal transduction. *Annu. Rev. Biochem.,* 69, 183–215.

[22] Koenig R.L., Ray J.L., Maleki S.J., Smeltzer M.S., Hurlburt B.K. (2004) *Staphylococcus aureus* AgrA binding to the RNAIII-*agr* regulatory region. *J. Bacteriol.,* 186, 7549–7555.

[23] Wuster A., Babu M.M. (2008) Conservation and evolutionary dynamics of the *agr* cell-to-cell communication system across firmicutes. *J. Bacteriol.,* 190, 743–746.

[24] Balagaddé F.K., Song H., Ozaki J., Collins C.H., Barnet M., Arnold F.H., Quake S.R., You L. (2008) A synthetic *Escherichia coli* predator-prey ecosystem. *Mol. Syst. Biol.,* 4(187), 1–8.

[25] Kambam P.K.R., Henson M.A., Sun L. (2008) Design and mathematical modelling of a synthetic symbiotic ecosystem. *IET Syst. Biol.,* 2, 33–38.

[26] Jabbari S., King J.R., Williams P. (2010) A mathematical investigation of the effects of inhibitor therapy on three putative phosphorylation cascades governing the two-component system of the *agr* operon. *Math. Biosci.,* 225, 115–131.

[27] Jabbari S., King J.R., Koerber A.J., Williams P. (2010) Mathematical modelling of the *agr* operon in *Staphylococcus aureus*. *J. Math. Biol.,* 61, 17–54.

[28] Jabbari S., King J.R., Williams P. Cross-strain quorum sensing inhibition by *Staphylococcus aureus*. Part 2: a spatially inhomogeneous model. *Submitted to Bull. Math. Biol. 2011,.*

[29] Jabbari S. Mathematical modelling of quorum sensing and its inhibition in *Staphylococcus aureus* PhD thesis University of Nottingham, UK (2007).

[30] Gustafsson E., Nilsson P., Karlsson S., Arvidson S. (2004) Characterizing the dynamics of the quorum-sensing system in *Staphylococcus aureus*. *J. Mol. Microbiol. Biotechnol.,* 8, 232–242.

[31] Cooksley C.M., Davis I.J., Winzer K., Chan W.C., Peck M.W., Minton N.P. (2010) Regulation of neurotoxin production and sporulation by a putative *agrBD* signaling system in proteolytic *Clostridium botulinum*. *Appl. Environ. Microb.,* 76, 4448–4460.

A   Model formulations

A.1   Model II - AgrA is constitutively phosphorylated

A.1.1   Dimensional model

The dimensional equations which change from (1)-(13) in Model II are (2), (12) and (13). Instead, Model II has

$$\frac{dA_j}{dt} \;=\; \kappa M_j + \phi A_{Pj} R_{Pj}^{a_j} + \mu A_{Pj} - (\psi_A + \delta_A) A_j, \tag{53}$$

$$\frac{dA_{Pj}}{dt} \;=\; \psi_A A_j - \phi A_{Pj} R_{Pj}^{a_j} - (\mu + \delta_{A_P}) A_{Pj}, \tag{54}$$

$$\frac{dP_j}{dt} \;=\; \frac{b}{N_j} A_j (1 - P_j) - u P_j, \tag{55}$$

with the initial conditions:

$$
\begin{aligned}
A_j(0) &= \frac{N_j \kappa m (\mu + \delta_{A_P})}{\delta_M ((\psi_A + \delta_A)(\mu + \delta_{A_P}) - \psi_A \mu)}, \\
A_{Pj}(0) &= \frac{\psi_A N_j \kappa m}{\delta_M (\psi_A + \delta_A)(\mu + \delta_{A_P}) - \psi_A \mu}, \\
P_j(0) &= \frac{b \kappa m (\mu + \delta_{A_P})}{b \kappa m (\mu + \delta_{A_P}) + u \delta_M ((\psi_A + \delta_A)(\mu + \delta_{A_P}) - \psi_A \mu)}.
\end{aligned}
\tag{56}
$$

A.1.2   Nondimensionalisation

We employ the same nondimensionalisation as for Model I, i.e. (15)-(20), and define the additional parameter:

$$\psi_A{}' = \frac{\psi_A}{\delta_M}.$$

A.2 Model III - AgrC is constitutively phosphorylated

A.2.1 Dimensional model

The dimensional equations which vary from (1)-(13) for Model III are

$$\frac{da_j}{dt} = kT_jS_j - \beta_{jj}R_{Pj}a_j + \gamma_{jj}(R_j^{a_j} + R_{Pj}^{a_j}) - \beta_{jl}R_{Pl}a_j + \gamma_{jl}R_{Pl}^{a_j} - \lambda_a a_j, \tag{57}$$

$$\frac{dR_j}{dt} = \alpha_R C_j - \psi_R R_j + \gamma_{jj}R_j^{a_j} - \delta_R R_j, \tag{58}$$

$$\frac{dR_{Pj}}{dt} = \psi_R R_j - \beta_{jj}R_{Pj}a_j + \gamma_{jj}R_{Pj}^{a_j} - \beta_{lj}R_{Pj}a_l + \gamma_{lj}R_{Pj}^{a_l} - \delta_{R_P}R_{Pj}, \tag{59}$$

$$\frac{dR_{Pj}^{a_j}}{dt} = \beta_{jj}R_{Pj}a_j - \phi A_j R_{Pj}^{a_j} - (\gamma_{jj} + \delta_{R_P^a})R_{Pj}^{a_j}, \tag{60}$$

$$\frac{dR_{Pj}^{a_l}}{dt} = \beta_{lj}R_{Pj}a_l - (\gamma_{lj} + \delta_{R_P^a})R_{Pj}^{a_l}, \tag{61}$$

$$\frac{dR_j^{a_j}}{dt} = \phi A_j R_{Pj}^{a_j} - (\gamma_{jj} + \delta_{R^a})R_j^{a_j}, \tag{62}$$

additional variables being required for this version of the *agr* model (see Table 1 for definitions of the various AIP-bound receptors and [26, 29] for more details).

The initial conditions which differ from (14) are

$$R_j(0) = \frac{N_j \alpha_R \kappa m}{\delta_M(\alpha_R + \delta_C)(\psi_R + \delta_R)}, \quad R_{Pj}(0) = \frac{N_j \psi_R \alpha_R \kappa m}{\delta_M \delta_{R_P}(\alpha_R + \delta_C)(\psi_R + \delta_R)}, \quad R_j^{a_j}(0) = 0, \quad R_{Pj}^{a_l}(0) = 0. \tag{63}$$

A.2.2 Nondimensionalisations

For Model III, as a result of the additional variables, we cannot simply adopt all the same nondimensionalisations as previously. The variable nondimensionalisations which change from (15) and (16) are thus

$$a_j' = \frac{\beta_{[11,22]}\phi b N_j \alpha_R \kappa^2 m^2 \psi_R}{\delta_M^5 \delta_A(\alpha_R + \delta_C)(\psi_R + \delta_R)\delta_{R_P}}a_j, \quad R_j' = \frac{\delta_M(\alpha_R + \delta_C)(\psi_R + \delta_R)}{N_j \alpha_R \kappa m}R_j,$$

$$R_{Pj}' = \frac{\delta_M \delta_{R_P}(\alpha_R + \delta_C)(\psi_R + \delta_R)}{N_j \psi_R \alpha_R \kappa m}R_{Pj}, \quad R_j^{a_j'} = \frac{b}{N_j \delta_M}R_j^{a_j}, \tag{64}$$

$$R_{Pj}^{a_l'} = \frac{\beta_{[22,11]}\phi b N_l \kappa m}{\beta_{[21,12]}\delta_M^3 \delta_A N_j}R_{Pj}^{a_l}.$$

The nondimensional parameters which change from (17)-(20) for Model III are

$$\lambda_X' = \frac{\delta_X}{\delta_M} = \lambda \quad \text{for} \quad X = A_j, T_j, R_j, S_j, R_{Pj}, R_{Pj}^{a_j}, R_{Pj}^{a_l}, A_{Pj},$$

$$\psi_R' = \frac{\psi_R}{\delta_M}, \quad k_a = \frac{k\beta_{11}\phi b \tilde{A}_1 \tilde{T}_1 \tilde{R}_{P1} \tilde{S}_1}{N_1 \delta_M^4}, \quad \beta_{11}' = \frac{\beta_{11}\tilde{R}_{P1}}{\delta_M}, \quad \beta_{21}' = \frac{\beta_{21}\tilde{R}_{P1}}{\delta_M}, \quad \zeta = \frac{b\tilde{R}_{P1}}{N_1 \delta_M}, \tag{65}$$

where $\tilde{X}$ is the initial condition of X given by (14) and (63) for $X = A_1, T_1, R_{P1}, S_1$.

B   Numerical investigations

B.1   Relative cross-inhibition binding rate, β_I

B.1.1   Model I

We here present some time-dependent solutions illustrating the various possible behaviours when $\beta_I = 180$ for Model I. Remember that this parameter choice enables either population to inactivate the other (Case Y from Table 4).

In Figure 20 we take the default initial conditions given by (38) for the first population and those for the second to be zero for all variables. We see how this initial advantage allows the first population to maintain the second in a down-regulated state, whilst upregulating itself. A slightly surprising result here is that the number of opposition-bound receptor in the first population is in fact higher than that of the second despite the fact that the first population is the active one (see $R_j^{a_l}$); this is because the number of unbound transmembrane AgrC is also much higher in the first population, so there is more available to attach to either AIP. A better comparison than between $R_1^{a_2}$ and $R_2^{a_1}$ is to compare the ratios $R_{P1}^{a_1}/R_1^{a_2}$ and $R_{P2}^{a_2}/R_2^{a_1}$, i.e. self-bound receptor to opposition-bound receptor. The final graph of Figure 20 shows that this is indeed higher for Population 1.

Figure 21 represents the solutions when we take the standard initial conditions, given by (38), for both populations. We see that despite the fact that they start in equivalent states with the exception that Population 1 has the advantage that the dimensional $\beta_{12} > \beta_{21}$ (so it has a faster rate of cross-species binding), the second population succeeds in forcing the first into an inactive state, achieving upregulation ($\bar{P}_2$ is much larger than $\bar{P}_1$ and $\bar{P}_2$ is close to unity). A possible interpretation of this is that β_{12} is so large that initially any available AIP from the first population binds to receptors of the second, resulting in more free AIP from the second population in the initial stages, allowing Population 2 to maximise its advantage and become up-regulated.

Finally, in Figure 22 we have taken the standard initial conditions for all variables except $P_1(0)$ which we have increased to $P_1(0) = 0.1$. This time, the solutions initially tend towards an inactive Population 1 and active Population 2. However, the slight extra strength of the first population gained through increasing its initial
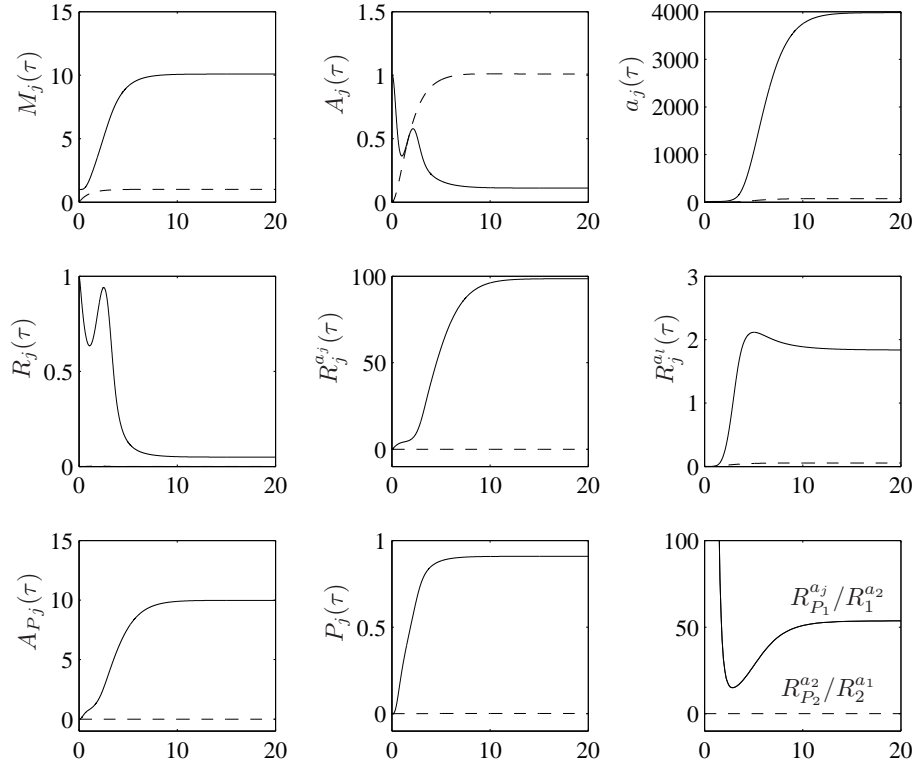
Figure 20: Time-dependent numerical solution to equations (22)-(37), i.e. Model I, for selected variables using the standard initial conditions, (38), for the first population (solid lines) and zero initial conditions for the second (dashed lines). $\beta_I = 180$ and all other parameters are taken from Table 3(a), meaning that the first population's inhibitory binding rate is faster than that of the second. The final graph illustrates the ratios of self-bound receptors to opposition-bound receptors for the two populations (the ratio for Population 2 is small, but positive, on this scale). Population 1 attains upregulation while maintaining Population 2 in an inactive state.
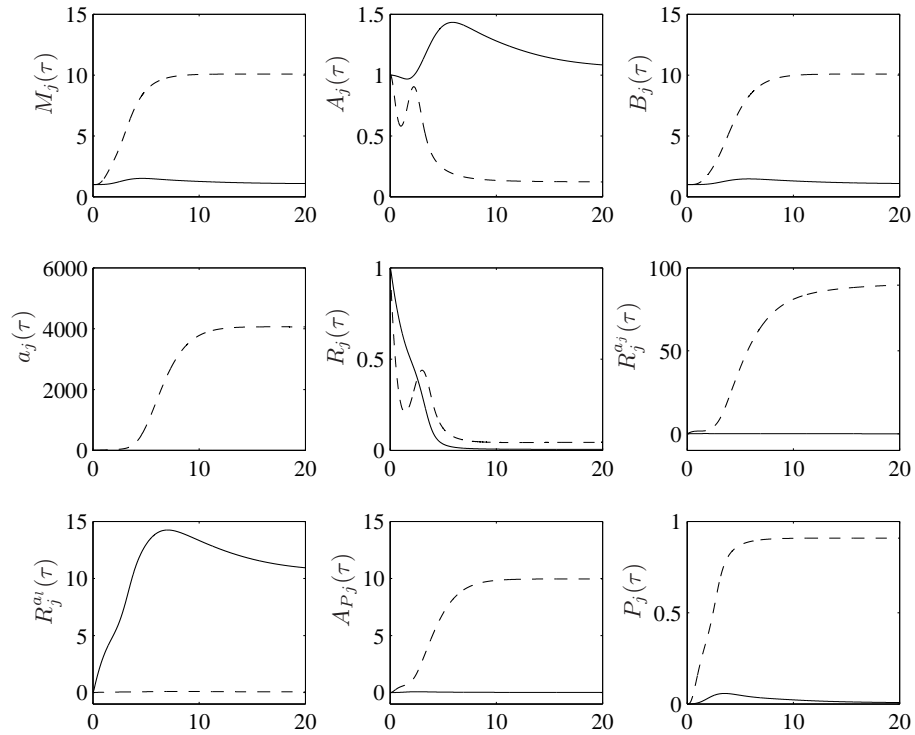
Figure 21: Time-dependent numerical solution to equations (22)-(37), i.e. Model I, for selected variables using the standard initial conditions given by (38) for both populations with $\beta_I = 180$ and all other parameters taken from Table 3(a). In spite of the fact that Population 1 (solid lines) has a higher inhibitory binding rate than Population 2 (and in all other respects the populations are equal), Population 2 suppresses Population 1.
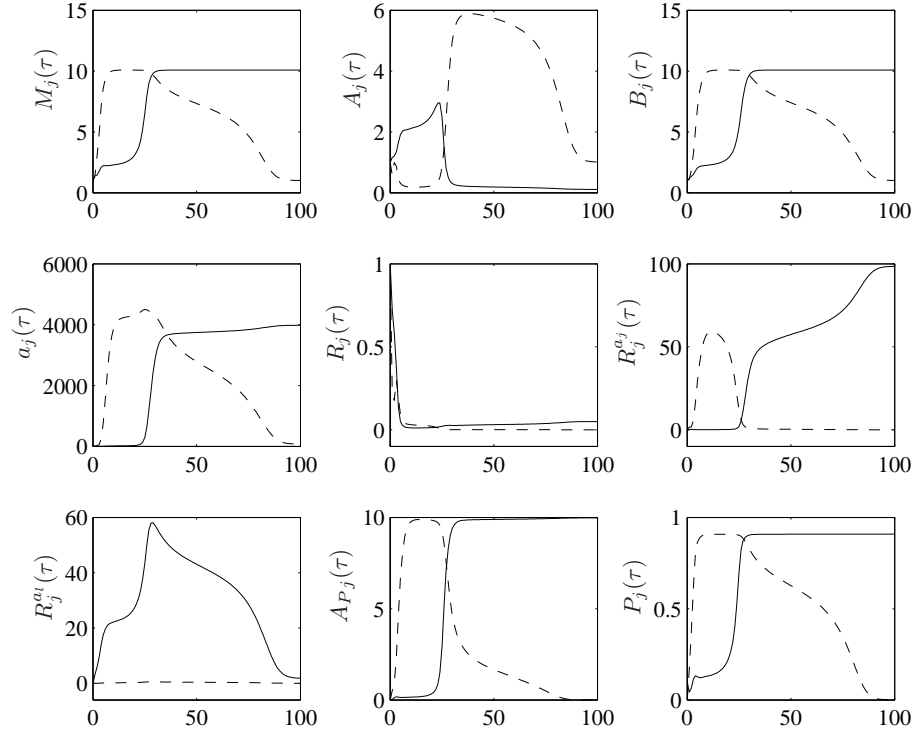
Figure 22: Time-dependent numerical solution to equations (22)-(37), i.e. Model I, for a selection of variables using all standard initial conditions, (38), except $P_1(0) = 0.1$. As for Figures 20 and 21, $\beta_I = 180$ and all other parameters are taken from Table 3(a). The higher level of initial activity in Population 1 (solid lines) enables it to achieve upregulation, simultaneously suppressing Population 2 (dashed lines).

level of activity enables it to produce enough AIP eventually to win the battle between the two populations and achieve a much higher level of up-regulation: $\bar{P}_1 >> \bar{P}_2$ (on [0 1]).